Dielectric and Magnetic Properties of Printed Wiring Boards and Other Substrate Materials

James Baker-Jarvis*, Bill Riddle *,
and Michael D. Janezic *

National Institute of Standards and Technology
325 Broadway, Boulder CO 80303-3328

This is an overview of dielectric and magnetic material measurements on printed wiring board and substrate materials. The most commonly used methods are presented. We begin with an overview of pertinent properties of circuit-board and substrate materials. We overview cavity and dielectric resonators, reentrant cavity, full-sheet resonance, coaxial probe, stripline, and capacitive methods. The frequency range of applicability and typical uncertainties associated with the methods are summarized. It is found that the reentrant cavity is useful for both loss and dielectric constant determination for materials of thickness greater than one-half millimeter. It is concluded that the full-sheet resonance technique is useful for the determination of the real part of the permittivity of clad substrates, but not for the loss measurement. Dielectric resonator techniques achieve the greatest sensitivity for both permittivity and loss. However, many printed wiring board materials are too lossy to achieve a resonance. We also present measurements of many substrate materials.

Key words: dielectric constant; dielectric resonator; full-sheet resonance; loss factor; microwave measurements; permeability; permittivity measurement; printed wiring board; resonance; stripline; substrate

*Radio-Frequency Technology Division, MS 813.01, email:jjarvis@boulder.nist.gov

1. Introduction

This report is an overview of the dielectric and magnetic properties of substrates and printed wiring board (PWB) materials. The goal of this report is to present relevant information on material properties and measurements for thin materials.

As electrical components are miniaturized, needs for accurate low-loss dielectric measurements on thin materials increases. There is a need for measurement metrology that supports the development of novel thin materials. Accurate measurement of complex permittivity and permeability are needed for circuit design, minimization of crosstalk, and characterization of propagation speed. As a consequence it is important to understand the related radio-frequency concepts and the limitations of the various measurement methods. In Section 2 we overview the important fundamental concepts in circuit-board applications. This includes the types of materials and laminates commonly used and the definitions of important electrical and thermal properties. We also provide an overview of the relevant concepts of transmission-line theory. In Section 3 we review the various permittivity methods for thin materials. In Section 4 we present measurements of substrate and circuit-board materials. In Section 5 we present a technique for elevated temperature measurements and measurement results for a number of commonly used materials.

2. Properties of Printed Wiring Board Materials

2.1. Overview of PWB Technology

New packaging technology requires low dielectric constant materials, interconnections made of high-conductivity metals, and high wiring density [1–9]. The use of fine-line signal conductors requires thinner, possibly laminated, low dielectric constant printed wiring board, thin films, and substrate materials. Monolithic integrated circuit applications require semiconducting substrate materials for active device operation.

The permittivity is written as $\epsilon = [\epsilon_r' - j\epsilon_r'']\epsilon_0$. The real part of the relative permittivity ϵ_r' is a measure of the phase change as a signal propagates through a material. The imaginary part of the permittivity ϵ_r'' is related to attenuation of the signal and includes both dielectric and d.c.-conductivity losses. Generally the loss in a material is expressed in terms of the loss tangent, $\tan\delta = \frac{\epsilon_r''}{\epsilon_r'}$. Dielectrics with low loss reduce attenuation and heating in circuits. In microelectronic applications the lower the dielectric constant, the

lower the propagation delay. This is manifest in the equation for propagation delay which is approximated by

$$t_d = \frac{l\sqrt{\epsilon_r'\mu_r'}}{c}, \tag{2.1}$$

where c is speed of light, l is line length, and μ_r' is the relative permeability given by $\mu = \mu_0[\mu_r' - j\mu_r'']$. Forming patterns or multilayers can decrease propagation delay by decreasing the signal path length. Propagation delay can also be decreased by lowering the dielectric constant; however, shortening the signal path increases wiring density and therefore increases cross-talk between elements. Low dielectric constant and anisotropy can decrease the signal cross-talk between conductors by decreasing the capacitive coupling.

High dielectric constant materials also have a niche in microelectronic applications. At low frequencies, well-characterized, high dielectric constant materials are used to keep dimensions of circuits small. This can be understood by considering how the TEM mode wavelength in a material λ is related to the permittivity and frequency f,

$$\lambda \approx \frac{c}{f\sqrt{\epsilon_r'\mu_r'}}. \tag{2.2}$$

Compact antenna arrays require high-dielectric constant substrates for maintaining phase shifts between elements. High dielectric constant materials include aluminum nitride, silicon carbide, polycrystalline alumina, monocrystalline materials such as quartz, sapphire, lanthanum aluminate, ferrimagnetic materials, titanates, and gallium arsenide [1].

Tunable or frequency-agile ferroelectric and ferrite materials in bulk or thin-film form are being used for device design and consequently a need for unbiased and biased dielectric and magnetic measurements. In ferroelectric materials the permittivity is a function of the applied bias field. In ferromagnetics or ferrimagnetics the permeability can be a function of the applied magnetic field. Permittivity tuning by applied voltage requires strong electric fields, so usually ferroelectric materials are used as thin-films. Ferroelectric materials such as barium-strontium titanate can be tuned by bias fields since the Curie temperature is close to room temperature. Domains consisting of electric dipoles are formed from strong dipole-dipole interactions. Ferroelectric material losses are affected strongly by temperature. The loss tangent of ferroelectrics increases approximately with temperature as T^2. Applications include phase shifters for antenna arrays. The loss in these materials is minimized by adding manganese to the solid. The most commonly used ferroelectric material is barium-strontium titanate. High-temperature performance of dielectric and ferromagnetic materials is also important for high-power systems.

Field orientation is important for measurements of anisotropic materials. The characterization of anisotropic materials generally requires two techniques, one for the component of permittivity perpendicular to the plane of the sample and one for in-plane permittivity.

Measurement fixtures in which the electromagnetic fields are tangential to the air-material interfaces, such as in TE_{01} cavities and dielectric resonators, generally yield more accurate results than fixtures where the fields are normal to the interface. Unfortunately, for many applications it is not always possible or preferable to measure in-plane field orientations. For example, circuit boards and printed wiring boards operate with the electric field primarily normal to the plane of the sheet and therefore this component of the permittivity is of primary interest. However, measurements with the electric field perpendicular to the sample face may suffer from consequences of air-gap depolarization. In such cases the air-gap must be either accepted, mitigated by metalization of sample surfaces or application of conductive pastes, or corrections made by numerical techniques [4,5].

For resonant measurements the permittivity or permeability is determined from measurements of the resonance frequency and quality factor (Q). The quality factor of a resonator decreases as frequency increases. This is a consequence of increasing loss as a function of frequency. In low-loss materials the permittivity is nearly constant over the microwave band. Many magnetic materials are low loss above magnetic resonance. In ferrite materials the permeability is a tensor for a bias field in the z direction is

$$\bar{\bar{\mu}} = \mu_0 \begin{pmatrix} \mu & j\kappa & 0 \\ -j\kappa & \mu & 0 \\ 0 & 0 & \mu_z \end{pmatrix}. \tag{2.3}$$

Since ferrites and garnets have magnetic-spin domains it is not possible to completely demagnetize a specimen. In the demagnetized state the permeability measurement yields μ_z. The gyromagnetic ratio and resonant (Larmor) frequency are related by $\gamma_g = -\omega_0/(\mu_0 H_0) = -1.759 \times 10^{11}$ m^2/Wb-s. As a magnetic field is applied to a specimen it reaches a level where all spins are aligned in the field. This is called saturation. The saturation magnetization M_s in ferrites is typically 0.03 T to 0.5 T. Below saturation ferrites are lossy, and as a consequence devices are usually operated at frequencies above saturation. The saturation field is strongly temperature dependent. Resonant systems with loss require a complex resonance frequency $\omega_0 \rightarrow \omega_0 + j\alpha\omega$. α is related to the linewidth, ΔH by $\Delta H = 2\alpha\omega/(\mu_0\gamma_g) = \Delta\omega_0/(\mu_0\gamma_g)$. Linewidth is a measure of the sharpness of the res-

Table 2.1. Summary of substrate properties and applications.

Property	Advantages	Desired range
Low dielectric constant	Minimize cross talk	$\epsilon_r' \approx 2-4$
	Decreased propagation delay	
High dielectric constant	Smaller circuits	$\epsilon_r' \approx 10-500$
	Generate phase changes	
Low loss	Less heat generated	$\tan\delta < 5 \times 10^{-4}$
	Less signal attenuation.	
Low thermal expansion	Less substrate fracturing	$\alpha < 10^{-5}(^oC^{-1})$
	Less impedance change with temperature	
High thermal conductance	Cooler operation	$k > 30$ (W/m^oC)

onance curve for the loss part of the magnetic susceptibility as a function of bias field strength.

Other important properties of printed wiring board and substrate materials include low loss, high thermal conductance, low thermal expansion, and high interfacial adhesion to metal surfaces or other films (see tables 2.1 and 2.2). Cost is a crucial for the widespread acceptance of a specific material. Epoxy-glass is the least expensive material and as a consequence holds a large market share. In increasing order of cost are epoxy-glass, polyimide,

Table 2.2. General properties of classes of PWB materials.

Class	Range of permittivity	Range of loss	TCE	Adhesion
Plastics	2 - 5	0.0001 - 0.01	poor	poor-good
Plastic/Ceramic composites	3 - 50	0.0001 - 0.01	good	poor-good
Glasses	3 - 12	0.00005 - 0.01	good	good
Ceramics	10 - 500	0.00005 - 0.01	good	good
Ceramic/Glass composites	4 - 100	0.00005 - 0.01	good	good

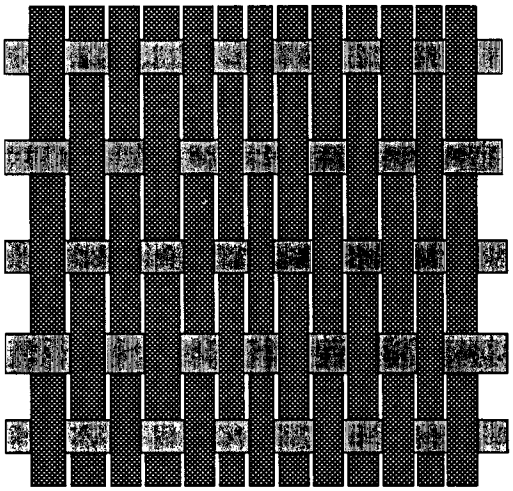

Figure 2.1. Typical reinforcing patterns used in PWB materials [10].

polyimide-quartz, and Teflon[1].

2.2. Materials Used in PWB and Substrate Applications

Printed wiring board and substrate materials are usually composite materials and may be anisotropic. The composites usually consist of a mixture of plastics and ceramics, together with reinforcing materials. Usually plastics are reinforced with glass fibers or impregnated with glass or ceramics. Typical reinforcing materials used are paper fabric, woven glass cloth, random fiberglass fibers, and aramid fiber cloth (see figures 2.1 and 2.2). The fabric and fiber weaving has some variability due to manufacturing limitations which translates into a variability in permittivity. Polymer resins are classified into thermoplastics or thermosets. Thermoplastics, for example polyethylene or Rexolite, soften when heated. Thermosets such as epoxies and phenolics do not melt when heated. Epoxies are polyethers and have good chemical resistance and adhesive properties. Common resins for low-cost laminates are phenolics. Phenolics, such as Bakelite, are thermosetting plastics. When heat and pressure are applied in the moulding process, thermosetting plastics react to form a

[1]Specific materials that are commonly used are mentioned. This does not imply any endorsement by the National Institute of Standards and Technology.

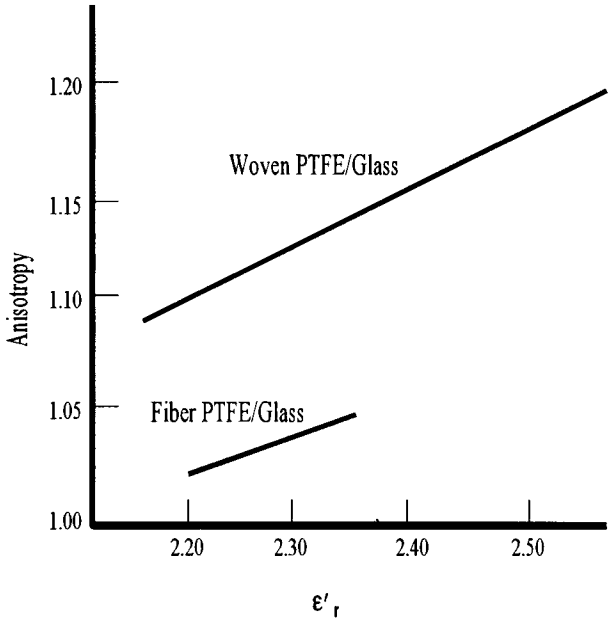

Figure 2.2. The degree of anisotropy in permittivity calculated from the ratio of normal to in-plane dielectric constant plotted against bulk dielectric constant [11].

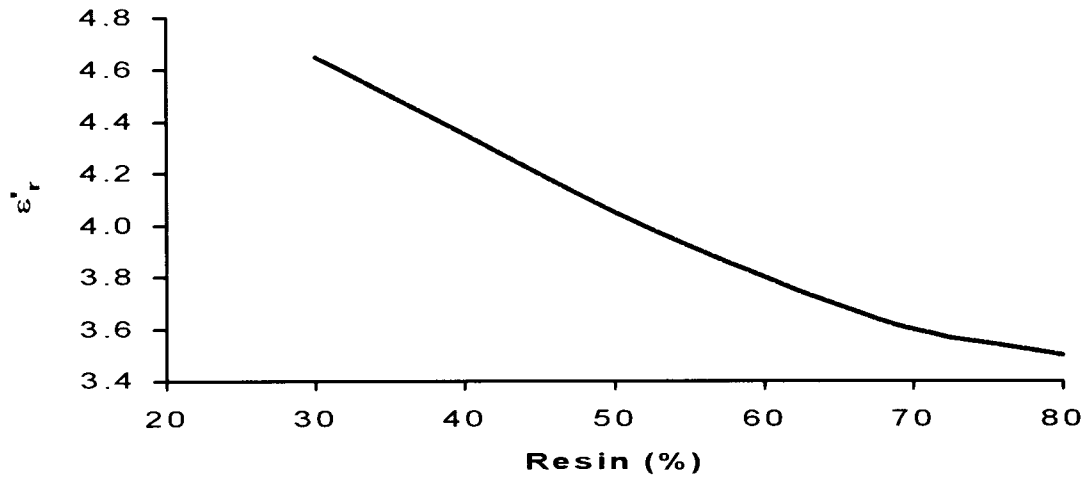

Figure 2.3. Dielectric constant in FR4 material as a function of the percent of resin content by weight [10].

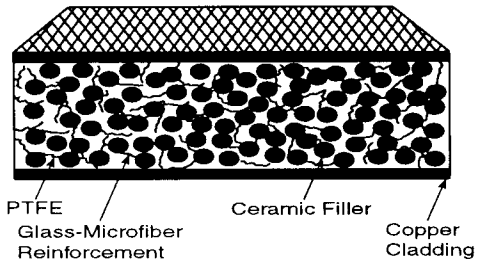

Figure 2.4. PTFE composite.

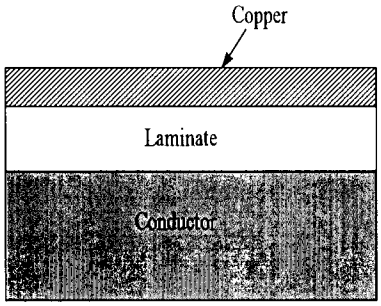

Figure 2.5. Geometry of metal-clad substrates.

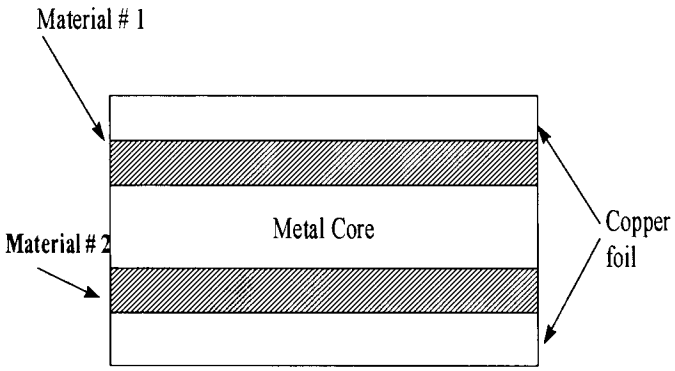

Figure 2.6. Dual material structure.

cross-linked structure. This structure yields excellent dimensional and thermal stability and superior load-bearing capability at low to high temperatures. Phenolic resins are products of the condensation reaction of phenol and formaldehyde. Other polymers used in PWB materials are polyimides, cyanate ester, bismalimide triazine (BT), fluropolymers, and polysulfone. Polyimides, bismalimide triazine, and cyanate ester can withstand higher temperatures than other polymers. Fluropolymers and polysulfone have low dielectric loss. Polymers may be crystalline, amorphous, or a combination. Dielectric properties as functions of both frequency and temperature of many commonly used organic materials are summarized in [12].

Many PWB's are laminates. Examples of laminates are fiberglass-epoxy composites (FR4), high-temperature fiberglass-epoxy composites (FR5), bismalimide triazine-epoxy, cyanate ester, arimid-epoxy, polyimide-glass, and polyimide-quartz [13] (see figures 2.1 through 2.6).

Low-dielectric constant materials include bulk plastics such as polytetrafluoroethylene (PTFE), cross-linked polystyrene (CPS), fiberglass, polyimides, fluropolymers, and composites made from fiberglass, fused silica, ceramics, aerogels, and foams. Plastics have low permittivities, but large expansion coefficients and low mechanical strength. Properties of plastic materials are summarized in table 2.3. Low-dielectric properties can be achieved by introducing porosity, use of low-dielectric constant materials, or by forming hollow stripline ceramic structures [14]. Recently, more complex low dielectric constant polymers such as polyquiolines and benzocyclobutenes have been developed.

Properties of some commonly used ceramics are summarized in table 2.4. Many ceramics such as alumina, aluminum nitride and silicon carbides have good thermal conductance, small expansion coefficient, and high dielectric constant. The ceramics beryllium oxide, aluminum nitride, and silicon nitride have higher dielectric constant than most organic materials and good mechanical strength [15,16]. The loss tangent for many ceramic materials and some plastics obey a linear dependence with frequency f of the form $\tan\delta = af + b$, where a is usually a positive number.

Sapphire, rutile, silicon, and quartz are anisotropic. Sapphire has a high thermal conductivity and very low dielectric loss. Sapphire and quartz are both brittle and difficult to drill and cut. Glasses such as fused silica and borosilicate have low loss and medium values of dielectric constants. Rutile has a very high dielectric constant and medium loss. Recently it has been shown that $Ba(Mg_{1/2}W_{1/2})O_3$ [17] and $Mg(Nb_xTa_{1-x})_2O_5$ [18] have

Table 2.3. Plastic substrates [1].

Material or composite	ϵ_r'	$\tan\delta$	Machinability	Range of temperatures (°C)	Anisotropy
PTFE	2.06	0.0002	Poor	-20 to 200	no
PTFE/Fiberglass	2.25	0.0010	Good	-20 to 200	yes
PTFE/Quartz	2.50	0.0005	Excellent	-20 to 200	yes
PTFE/Ceramic	10.0	0.0010	Excellent	-20 to 200	yes
CPS	2.54	0.0004	Good	-20 to 100	no
CPS/Fiberglass	2.70	0.0010	Good	-20 to 100	yes
CPS/Quartz	2.70	0.0005	Good	-20 to 100	yes
Polyolefin	2.30	0.0005	Poor	-20 to 100	no
Polyimide	3.50	0.0010	Good	-20 to 200	no

high-dielectric constant, low loss, and low coefficient of thermal expansion. Zirconium titanate with added ZnO, Y_2O_3, or CuO has been shown to have low expansion coefficient, high dielectric constant and low loss [19]. Another well-studied high-dielectric constant ceramic is $Ba(Zn_{1/3}Ta_{2/3})O_3$. The presence of tantalum increases cost. It has been found that if this material is doped with $BaZrO_3$, the domain boundaries are stabilized and losses decrease [20]. A novel high-permittivity material $AgNb_{1-x}Ta_xO_3$ with dielectric constant in the 300 to 400 range with losses on the order of $\tan\delta \approx 1 \times 10^{-3}$ has been developed [21,22]. Semiconducting materials such as silicon and gallium arsenide are also used as substrates. Silicon is very lossy at low frequencies, whereas gallium arsenide is low loss over the microwave band.

Examples of dielectric resonators used in the wireless industry as shown in figure 2.7 are made of low-loss, temperature stable, high-dielectric constant materials. The requirements for dielectric resonators are summarized in table 2.5. Dielectric resonators are used as oscillators, filters for rejection of unwanted frequencies, and combiners. Materials commonly used for high-Q resonators include alumina, sapphire, and titanate compounds. The relevant properties of dielectric resonators are summarized in table 2.5.

Magnetic substrates include garnets and ferrites. Loss-loss magnetic materials are used in isolators and circulators. A commonly use magnetic substrate is yttrium-iron garnet

Table 2.4. Ceramic substrates [1].

Material or composite	Machinability	Range of temperatures (^{0} C)	Anisotropy
Alumina	Good	-200 to 300	no
Sapphire	Fair	-200 to 300	yes
Fused silica	Good	-200 to 500	no
Rutile	Good	-200 to 500	yes
Beryllium oxide	Good	-100 to 300	no
Aluminum nitride	Good	-200 to 300	no
Borosilicate/Alumina	Good	-200 to 500	yes

Table 2.5. Summary of important properties for dielectric resonators.

Property	Advantages
High-dielectric constant	Miniaturization
Low loss	Large Q, close channel spacing
Low-thermal expansion	Frequency stability
High-thermal conductance	Cooler operation

(YIG).

2.3. Thermal Properties

The two thermal properties relevant to substrates are coefficient of thermal conductivity (k) and thermal coefficient of expansion (TCE). The thermal coefficient of expansion α_{TCE} is defined as

$$\alpha_{\text{TCE}} = \frac{\Delta L}{L\Delta T}, \tag{2.4}$$

where L is material thickness and ΔL is change in thickness as temperature changes by ΔT. Coefficients of thermal expansion are given for a number of materials in table 2.6 [1, 16,23,25]. Most materials have positive temperature coefficients of permittivity. There are exceptions to this rule. Materials with negative temperature coeficients can be combined

Table 2.6. Thermal coefficients of expansion (TCE).

Material	$\alpha \times 10^6$ ($^oC^{-1}$)	Material	$\alpha \times 10^6$ ($^oC^{-1}$)
ABS plastic	71	lanthanum aluminate	9
acetal	85	lithium niobate	15 $\perp$, 4.1 $\parallel$
acrylic	68	magnesium oxide (MGO) [1]	8
alumina [1]	6.7	neodymium gallate	9
aluminum [1]	24	nylon	90.7
aluminum nitride [1]	4.6	PMMA	68
aluminum oxide [1]	2.6	polycarbonate	66
aluminum titanate	0.4	polyethylene (high density)	129
aramid/epoxy [10]	6-9	polyimide [23]	40
beryllium oxide [1]	8.5	polyimide/glass [1]	14-15
bismalimide triazine/epoxy [10]	15-17	polyimide/quartz [10]	6-8
borosilicate glass [23]	3.1	polypropylene [24]	86
calcium oxide	14.8	quartz [1]	11.2
copper [1]	17	Rexolite [6]	70
cordierite [1]	1.0	rutile [1]	70
cyanate ester [10]	13	sapphire [1]	5.3
diamond [1]	1.02	silicon [1]	3
epoxy [24]	54	silicon carbide [1]	3.7
FR-4 [1]	17-18	spinel [1]	6.6
FR-5 [1]	17-18	strontium titanate	9
fused quartz	0.5	strontium lanthanum aluminate	7 [6]
fused SiO_2	0.5	strontium lanthanum gallate	10 [6]
fused silica [1]	0.5	Teflon [6]	140
gallium arsenide [6]	5.7	tridymite [1]	17.5
gallium gadolinium garnet	8	zirconia oxide	9.2
germanium	6.1	Zr-Sn titanate [1]	-6.9
kovar	5		

Figure 2.7. Dielectric resonators.

with materials with positive temperature coefficients to produce a material with small composite change with temperature. Plastics have large TCE and low glass transition temperatures T_g (see table 2.7).

The temperature coefficient of permittivity is defined as

$$\tau_\epsilon = \frac{1}{\epsilon_r'} \frac{\Delta \epsilon_r'}{\Delta T}. \tag{5}$$

τ_ϵ is usually expressed in parts in 10^6 [?]. The temperature coefficient of permittivity is usually evaluated at constant pressure rather than constant volume. The effects of temperature on permittivity has two origins. One is thermal expansion which is due to lattice size changes and the other is the change of the lattice with temperature.

A commonly used method of quantifying the effects of temperature on resonance frequency is the temperature coefficient of resonance frequency

$$\tau_f = \frac{\Delta f}{f} \frac{1}{\Delta T}. \tag{6}$$

The thermal coefficients of expansion for composites can be calculated by mixture formulas such as

$$\alpha_{\text{eff}} = \frac{\sum_i \alpha_i k_i V_i}{\sum_i k_i V_i}, \tag{7}$$

Table 2.7. Glass transition temperature [10].

Material	T_g (°C)
Polyimide/Quartz	250
Cyanate ester	250
Polyimide/Glass	250
Teflon	200
BT/Epoxy	190
FR5	170
Rexolite	120
FR4	130

where k_i, α_i, and V_i are the bulk modulus, coefficient of expansion, and volume fraction of the *ith* phase [27]. The effective dielectric constant of a mixture of constituents with permittivity ϵ_{ri} can be approximated by [27]

$$\frac{\epsilon'_{r(eff)} - 1}{3\epsilon'_{r(eff)}} = \sum_i \frac{V_i(\epsilon_{ri} - 1)}{(\epsilon_{ri} + 2\epsilon_{r(eff)})}. \tag{2.8}$$

In addition to thermal expansion there is the problem of thermal warping of circuit boards. Warping or camber is a result of differential thermal expansion. A measure of camber can be estimated by

$$\frac{\Delta W}{L} = \frac{\alpha_w L \Delta T}{d}, \tag{2.9}$$

where ΔW is the height of the warp of the material from a plane surface, α_w is coefficient of thermal bending, L is the length of material, and d is thickness [28].

2.4. Electric Properties of Surface-Cladding Material

Clad materials can have appreciable surface roughness. In order to promote adhesion, the copper foil that is applied to the PWB material has a roughened surface. Surface roughness affects measured capacitance. The effect of surface roughness on the loss tangent is small at low frequencies; however, above 1 GHz the resistance of rough copper increases over

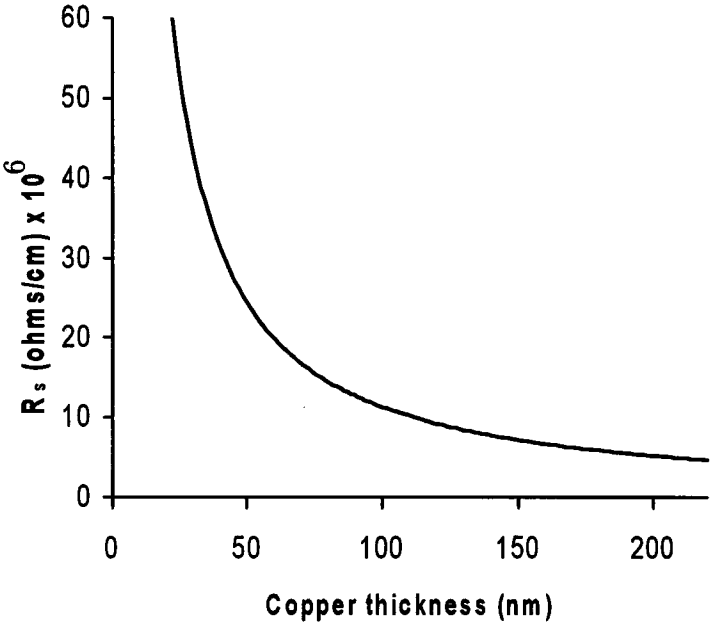

Figure 2.8. Copper thickness versus resistance [10].

Table 2.8. Conductivities of metals.

Material	Conductivity, σ /10^7 (S/m)	Skin depth at (10 GHz) /10^{-7} (m)
Cu	5.80	6.60
Al	3.72	8.26
Ag	6.17	6.42
Au	4.10	7.85
In	0.87	17.0
70-30 brass	1.57	12.70
Typical solder	0.71	19.0

that of smooth copper [2]. Fields may penetrate thin metal cladding (see figure 2.8). The skin depth is related to the conductivity σ by

$$\delta = \frac{1}{\sqrt{\pi f \mu \sigma}}. \tag{2.10}$$

The surface resistivity is

$$R_s = \sqrt{\frac{\pi f \mu}{\sigma}}. \tag{2.11}$$

Electrical conductances of commonly used metals are given in table 2.8.

2.5. Transmission-Line Parameters for Circuit-Board Applications

Important properties of transmission lines in PWB applications are attenuation, loss, phase, impedance, and propagation delay. The propagation constant is given in terms of distributed-circuit parameters fot $R \ll \omega L$

$$\gamma = \alpha + j\beta = \sqrt{(R + j\omega L)(G + j\omega C)}, \tag{2.12}$$

where C, G, L, R are measured distributed circuit parameters per unit length. In eq (2.12) we neglected the term containing CG and R is total resistance per unit length. For TEM waves the attenuation can be separated into conductor and dielectric components

$$\alpha_p = \frac{R}{2Z_0} + \frac{\omega}{2}\sqrt{\frac{\mu_0 \mu_r'}{\epsilon_0 \epsilon_r'}}\epsilon'', \tag{2.13}$$

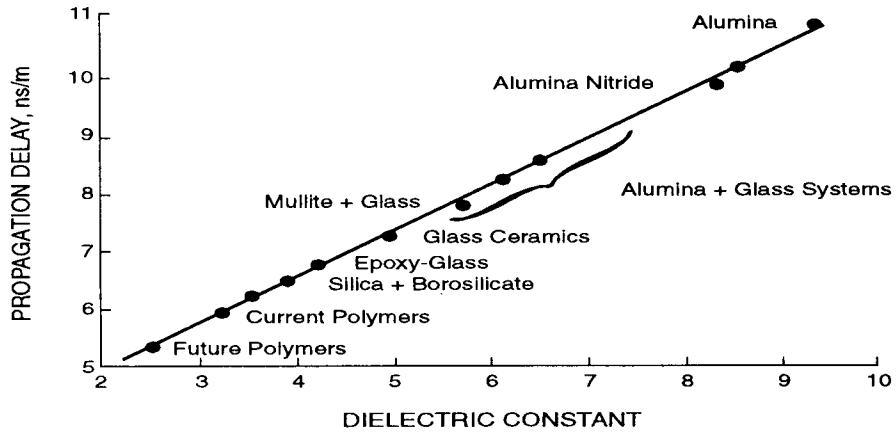

Figure 2.9. Propagation delay versus dielectric constant for many materials with RC circuit where Z_0 is the characteristic impedance of the line and R_t is series resistance.

The characteristic impedance is

$$Z_0 = \sqrt{\frac{R + j\omega L}{G + j\omega C}}. \tag{2.14}$$

The loss tangent is $\tan\delta = G/(2\pi f C)$. The propagation delay/m in a lossless line is

$$t_d = \sqrt{\epsilon_r' L C_{vac}}, \tag{2.15}$$

where L and C_{vac} are the inductance and vacuum capacitance of the line. The propagation delay increases as the square root of the dielectric constant [23]. In figure 2.9 the propagation delay is plotted against the dielectric constant.

Table 3.1. Measurement parameters.

Component of permittivity (in-plane or normal)
Frequency
Loss measurement
Specimen thickness
Temperature

3. Dielectric Measurements

3.1. Overview of the Measurement Problem

No single technique can characterize all materials over all frequencies. Each frequency band and loss regime requires a different method. Thin materials present a unique measurement challenge since thickness is the dominant source of uncertainty for many measurements. Dielectric properties depend on frequency, homogeneity, anisotropy, temperature, surface roughness, and in the case of ferroelectrics, applied d.c. bias field [2]. Dielectric materials may be isotropic or anisotropic, epitaxial or amorphous, clad or unclad. Anisotropy is usually a result of weaving fiber in the material. In table 3.1 some of the various parameters pertaining to permittivity measurements are summarized. The measurement of thin materials presents a special challenge in that uncertainties in thickness of the specimen translates into uncertainty in the permittivity.

3.2. Measurements of Thin Materials

3.2.1. Measurement Methods

In this section we will overview the most commonly used thin material measurement techniques. We will discuss and compare the strengths and weaknesses of each technique. We will also compare the techniques in light of destructive versus nondestructive measurements. For each technique, we either overview the theory or we refer to published work [29]. We will indicate which fixtures can be used for obtaining permittivity normal or in the plane of the sample. We also will give an uncertainty range for each fixture. We do not consider thin films since this is an extensive area in and of itself. For thin films we

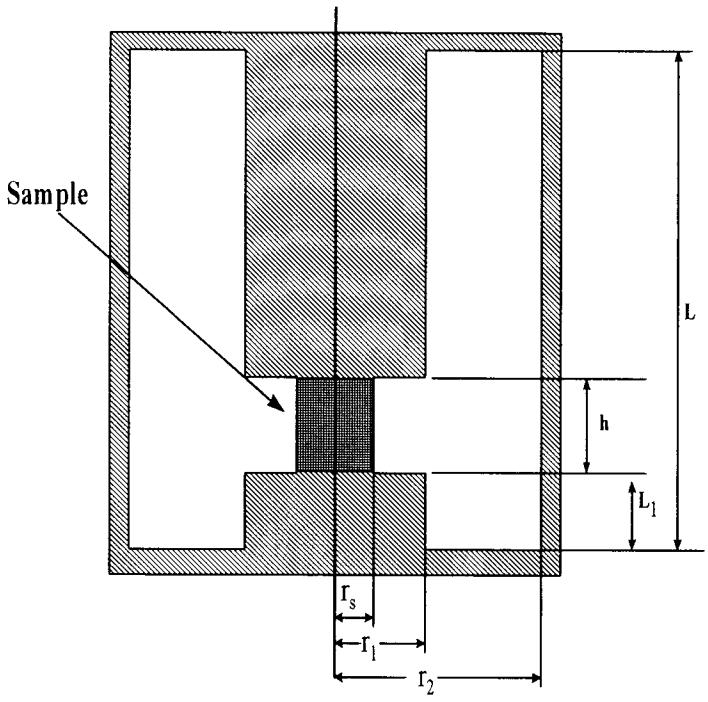

Figure 3.1. Schematic cross section of the reentrant cavity. The coaxial line inner and outer diameters are $2r_1$ and $2r_2$, and specimen diameter is $2r_s$ as indicated. The cavity height is L.

refer the interested reader to recent references [30, 31].

3.2.2. Reentrant Cavity

Resonant measurement methods are the most accurate ways of obtaining dielectric constant and loss tangent. Most resonant techniques yield permittivity in the plane of the sample. The resonant reentrant cavity is an exception in that it yields the permittivity component normal to the face of the material at radio frequencies. The reentrant cavity is useful because it is possible to accurately measure materials at frequencies from 100 MHz to 1 GHz.

The reentrant cavity depicted in figure 3.1 consists of a coaxial line or other transmission line with a gap in the inner electrode. The specimen is inserted into this gap. The cavity is then resonated and the capacitance of the gap produces a frequency shift. If the specimen

gap region is at the very top or bottom of the cavity then the system is called a *singly reentrant cavity*, whereas, if the sample gap is in the middle of the cavity it is called a *doubly reentrant cavity*. The loss tangent is determined from quality-factor measurements with and without specimen in place. Typical uncertainties for a well-characterized system for low to medium permittivity are $\Delta\epsilon_r' = \pm 1\%$, $\Delta \tan\delta = \pm 0.0005$.

Two approaches have been used for modeling the reentrant cavity. The first is a lumped-circuit approximation [32,33]. The other approach is a rigorous mode-matching technique [34–36]. The full-field model is given in reference [34].

3.2.3. TE_{01} Split-Cavity Resonators for Thin Dielectrics

Unclad thin materials can be measured nondestructively using a split-TE_{011} cavity resonator as depicted in figure 3.2 [37–39]. This dielectric-resonator technique allows rapid measurement at X-band frequencies for thin, low-loss materials. This type of resonator has the electric field in the plane of the sample. The thin material is placed between the sections and a resonant mode is excited. Generally the cavity is operated such that the $TE_{01\delta}$ mode propagates in the specimen and is evanescent outside the specimen. These cavities can be constructed in various sizes to allow operation at frequencies from 8 to 20 GHz. Typical uncertainties are $\Delta\epsilon_r' = \pm 0.2\%$ and $\Delta \tan\delta = \pm 5 \times 10^{-5}$. The theory for

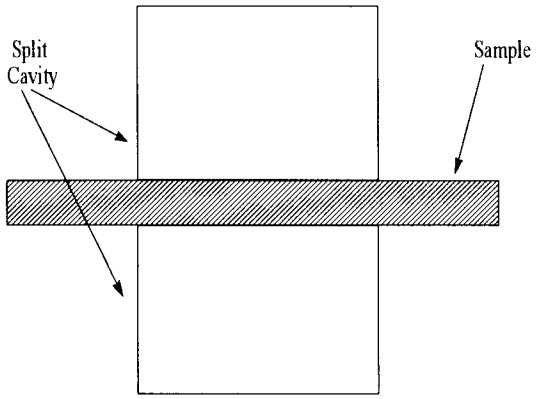

Figure 3.2. TE_{01} split-cavity dielectric resonator for thin sheets.

this fixture is summarized in references [37,38]. Details of the full-mode model are given in reference [40]. The full-mode model includes the effects of the fringing fields at the gap in the cavity.

3.2.4. Cavity Resonators for Thin Dielectrics

Cavities have also been used for thin materials. The most common cavity is the TE_{01} resonator [41]. In this case the permittivity in the plane of the specimen is measured. The TM_{0m} cavity is also commonly used. In this cavity there is a strong E_z component of the electric field at the center. If a specimen is placed near the center then it is possible to measure the E_z component of the permittivity [42]. Either rod or bulk specimens can be used. TM_mn0 cavities have been used to measure the components of the permeability tensor. In these measurements a thin rod specimen is inserted in a hole at the center of the cavity [43]. A rod specimen has an advantage of less demagnetization.

3.2.5. TE_{01} Split-Post Dielectric and Magnetic Resonators

The split-post dielectric and magnetic resonator techniques are methods for measurement of thin materials (see figures 3.3 and 3.4) [44–46]. In the split-post method a thin material or film is inserted between two fixed dielectric resonators. The posts which support the resonators have low dielectric constant and low loss. The resonance frequency and quality factor of the posts are influenced by the presence of the specimen. Split dielectric resonators were developed by DelaBalle [47,48], Maj [46], and Nishikawa et al. [45]. There are many variations of this technique reported in the literature. Some fixtures have the specimen extending to the back wall of the cavity. The lowest-loss technique is when the dielectric resonators are supported by low dielectric constant posts. This configuration has the advantage of reduced wall loss. Nishikawa et al. [45] used the finite element method to analyze this fixture. Various techniques have been employed for this purpose: finite difference , mode-matching, and finite-element methods. The geometry of a split dielectric resonator fixture used in our measurements is shown in figure 3.3. Such a resonator operates with the $TE_{01\delta}$ mode which has only an azimuthal electric field component so that the electric field remains continuous on the dielectric interfaces. This minimizes air gap systematic uncertainties. The resonator measures the permittivity component in the plane of the specimen. A useful feature of the split-post resonator is that it can be designed to operate in the low gigahertz region. We have successfully used dielectric resonators

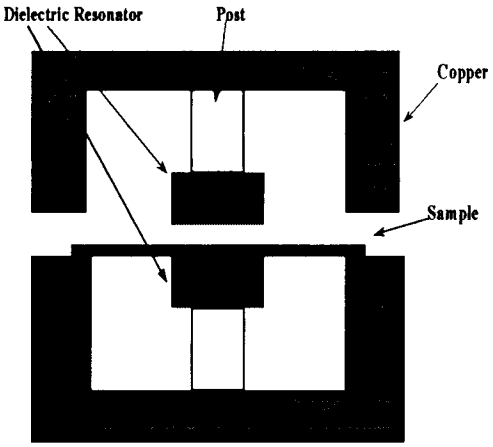

Figure 3.3. Schematic diagram of a split dielectric resonator fixture.

operating from 1.5 to 12 GHz. Loop coupling is used in these dielectric resonators.

Thin magnetic materials can be measured with the split-post magnetic resonator technique. This fixture consists of a dielectric post above a ground plane. The ground plane induces a region of strong magnetic field. The thin magnetic material is inserted between the posts and resonance frequency and quality factors are measured. This technique is combined with the split post to solve similtaneously for both ϵ and μ.

The main source of uncertainty in the real part of the complex permittivity of the split-post resonator, as with the split-cavity resonator measurement, is from the uncertainty in the thickness of the specimen. The relative uncertainty of the real part of the permittivity is primarily due to thickness uncertainty. We have found the following equation for a specimen of thickness h is useful to estimate uncertainties

$$\frac{\Delta\epsilon_r'}{\epsilon_r'} = 2\frac{\Delta h}{h}. \tag{3.1}$$

Typical uncertainties in the split-post resonator of the real part of permittivity are $\Delta\epsilon_r' = \pm 1\%$. Dielectric loss tangent uncertainty depends on other factors such as the accuracy with which the quality-factor can be measured. For properly chosen specimen thickness, it is usually possible to resolve dielectric loss tangents to approximately $\pm 5 \times 10^{-5}$ for quality-factor measurements made with accuracies of 1 %.

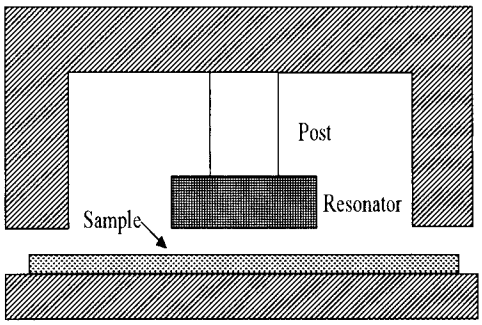

Figure 3.4. Schematic diagram of a split magnetic resonator fixture.

3.2.6. Courtney Technique

The Courtney fixture can be used to measure the dielectric properties of materials at gighertz frequencies [26, 49–54]. In this technique the $TE_{01\delta}$ mode is used to determine dielectric properties. Low-loss, high dielectric constant sleeves are used to lower the resonance frequency, thereby increasing the frequency coverage. Two measurements are required to get both the permittivity and permeability of a material. First the material may be measured without an applied magnetic field and then the Courtney fixture can be placed between the poles of a magnetic so that the permeability can also be measured. In figure 3.6 we show a Courtney fixture with a specimen and sleeve resonator. Measurements on garnets are given in figure 3.5 [49]. These measurements were made using both a TE_{011} resonator with sleeves and a coaxial transmission-line technique.

3.2.7. Full-Sheet Resonance Method for Thin Sheets

The full-sheet resonance technique is used to determine the permittivity of clad circuit and printed wiring board materials (see figure 3.7) [55–57]. It is a nondestructive test and measures the bulk property of a substrate. The frequency of measurement is limited by the specimen dimensions since the method uses one-half wavelength resonances. The

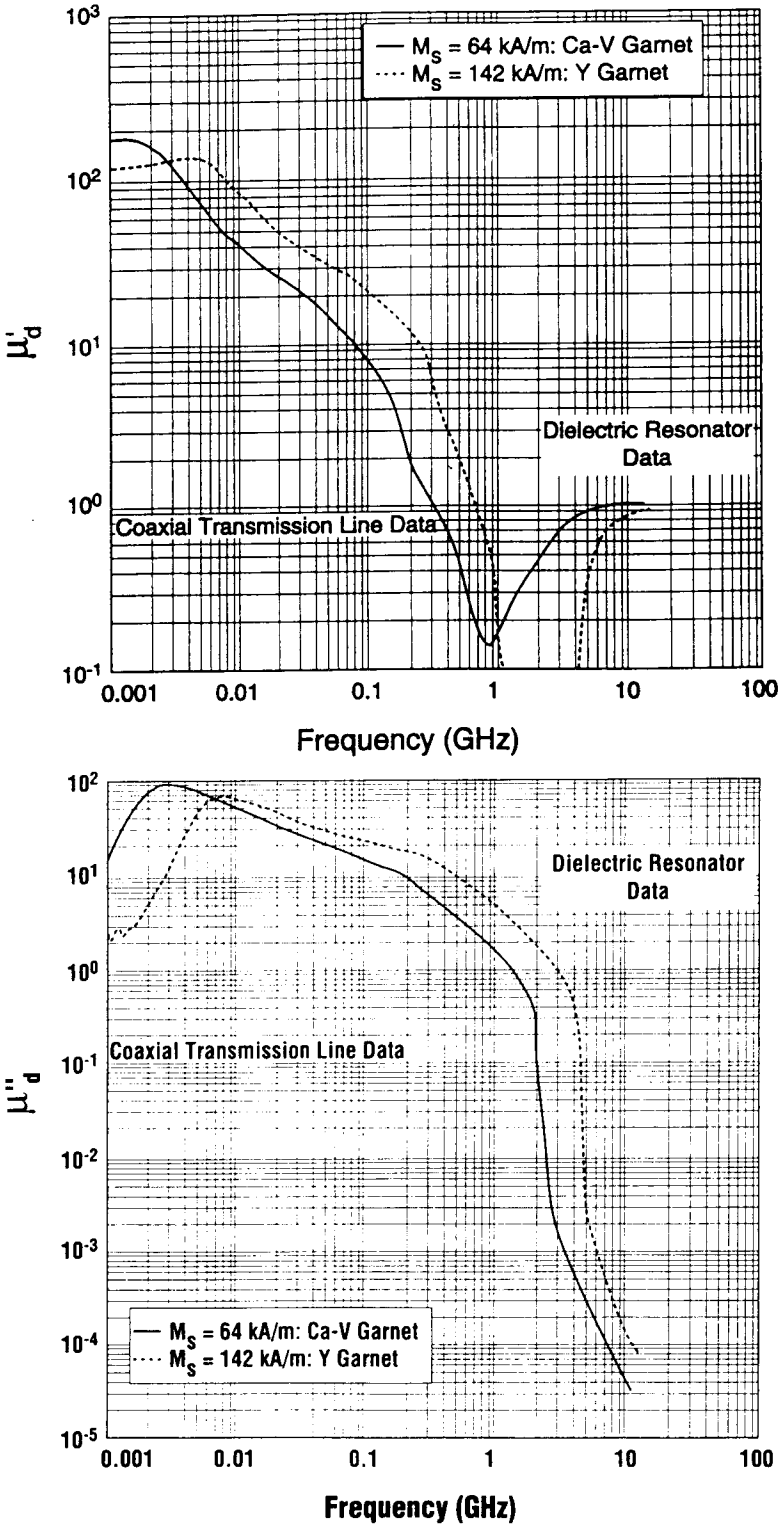

Figure 3.5. Measurements on demagnetized garnets [49].

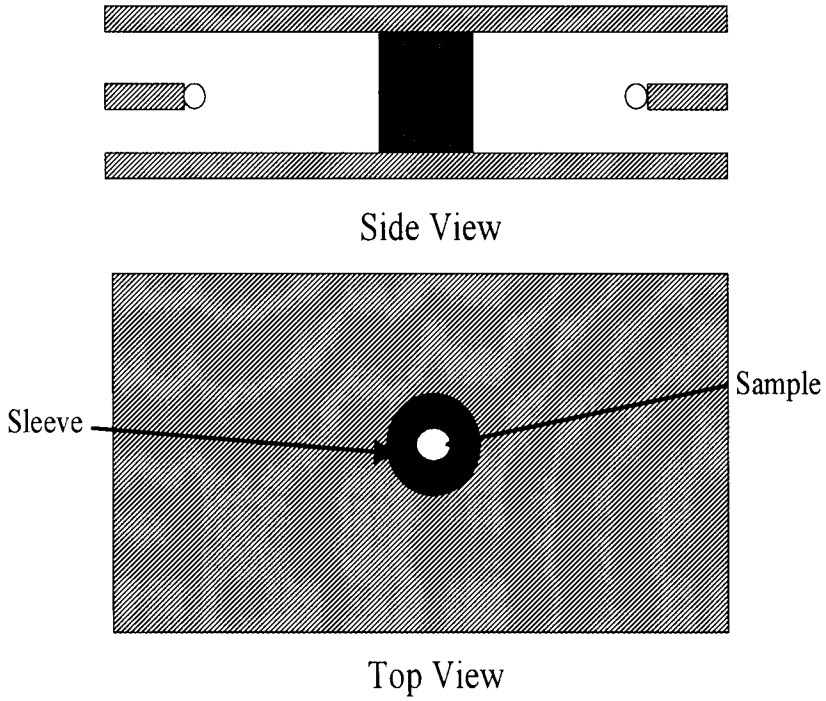

Figure 3.6. Courtney fixture with dielectric sleeve.

specimen is usually open at the sides; however some researchers measure with the sides closed. The open edges make the electrical length of the specimen slightly longer than the actual physical dimensions. The permittivity is measured by transmission and reflection coefficients of test signals introduced by coupling to coaxial feeds. This causes the cladded structure to resonate at integral multiples of one-half wavelength in the specimen. Higher modes can also be used to extend the frequency coverage. The main difficulty in this technique is mode identification and degeneracy. The full-sheet resonance method is limited in its ability to determine the loss factor since the surface area of the metal cladding is large relative to the volume of the specimen.

The relative permittivity is obtained from the resonant frequencies of a cavity. The resonance condition for TE_{mn} modes is

$$\epsilon_r' = \left(\frac{c}{2f_{mn}}\right)^2 \left[\left(\frac{m}{a}\right)^2 + \left(\frac{n}{b}\right)^2\right], \tag{3.2}$$

where c is speed of light, and a and b are cross sectional dimensions, m and n are mode

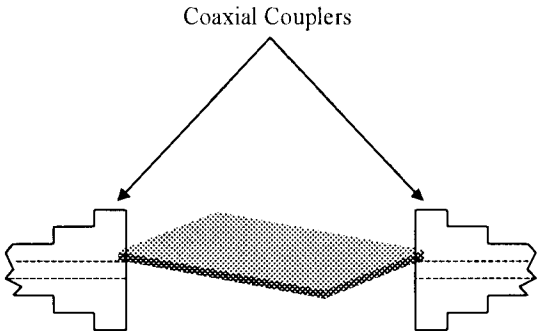

Figure 3.7. Full-sheet resonance technique

numbers, and f_{mn} are the resonant frequencies. Note that the equation does not depend on specimen thickness. This lack of sensitivity to thickness has an advantage over other techniques.

The measured resonant frequencies calculated from eq (3.2) differ from the theoretical frequencies because of the open edges, conductivity of the plates, and radiation losses. The very low measured quality factors in this technique produce frequency-pulling that must be taken into account. Mode interference can also be a problem. Generally, better mode separation is possible if the specimen is rectangular rather than square.

Collins derived an expression that accounts for frequency pulling due to finite wall conductivity

$$f_l = f_{ul}\sqrt{1 + \frac{1}{Q_c} + \frac{B_R}{G_R Q_R}}, \tag{3.3}$$

where f_l and f_{ul} refer to loaded and unloaded resonant frequency. Q_R is the radiation quality factor, and $Y_R = G_R + jB_R$ is the open-side aperture impedance [55].

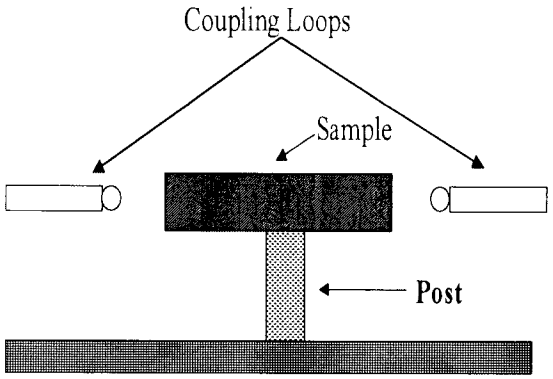

Figure 3.8. Whispering gallery mode resonator. The specimen is in form of a disk.

The quality factors of cavity, radiation, and coupling ports Q_C, Q_R, and Q_e are related to the loaded Q_L

$$\frac{1}{Q_L} = \frac{1}{Q_C} + \frac{1}{Q_R} + \frac{1}{Q_e} = \frac{1+\kappa}{Q_0}, \tag{3.4}$$

where κ is the cavity coupling coefficient.

The real part of the permittivity is also affected by the open sides of the specimen. A correction for open sides can be made in terms of the capacitance of the plates C and fringing capacitance C_f.

The relative permittivity with end correction is obtained from the resonant frequencies of a cavity. The resonance condition is

$$\epsilon_r' = \frac{C + C_f}{C + C_f/\epsilon_r'} \left[\frac{c}{2f_{mn}}\right]^2 \left[(\frac{m}{a})^2 + (\frac{n}{b})^2\right]. \tag{3.5}$$

3.2.8. Whispering-Gallery and Fabry-Perot Resonators

Low-loss dielectric and magnetic materials can be measured in the microwave frequency range by use of whispering-gallery modes as shown in figure 3.8 [58–61]. Whispering-gallery modes have been used in measurements of both the real part of the permittivity and loss tangent. Highly accurate dielectric loss measurements can be made using this technique. In this dielectric-resonator technique the specimen is usually supported from the bottom

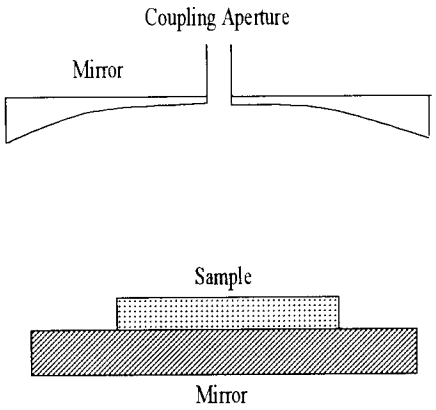

Figure 3.9. Fabry-Perot resonator.

with a dielectric rod. The support rod does not influence the measurement because the modes do not penetrate appreciably into the specimen [47,57,62–66]. Measurements using whispering-gallery modes on low-loss materials are advantageous since conductor loss can be made very small.

Open resonators have been used for measuring low-loss materials in the millimeter range in the configuration shown in figure 3.9 [67–71]. Open Fabry-Perot resonators consist of two separated mirrors with a coupling aperture on one of the mirrors. In the confocal setup both mirrors are concave, whereas in the semi-confocal arrangement one of the mirrors is flat and the other is concave. The concave feature of the mirror minimizes radiation leakage from the open sides of the resonator and focuses the beam onto a smaller area of the specimen under test, thereby minimizing specimen edge diffraction effects. Fabry-Perot resonators have large quality factors and are useful for measurements on thin, low-loss materials. Since they are open structures they suffer from radiation leakage. The tensor permittivity values can be obtained by measuring at different angles of incidence. The metal in the mirrors limits the accuracy of the loss measurement. Thin substrate materials can be measured with this technique by positioning the specimen on the flat mirror.

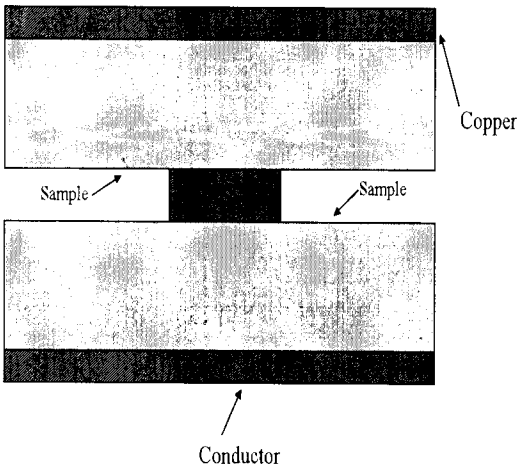

Figure 3.10. Stripline resonator [11].

3.2.9. Transmission-Line Techniques

Various transmission-line techniques have been used for nondestructive substrate property determination [41, 72–78]. These techniques can be broadly grouped under resonant or nonresonant techniques. In many applications transmission lines have open surfaces. Open structures can radiate and have a more complicated field structure [3, 79–93]. Conductors may be deposited directly on wiring boards or substrates to form transmission lines, or alternately, the conductor on a PWB board may be etched or routed into a test fixture. PWB materials are thin and usually clad by copper, making measurements with closed waveguide or coaxial transmission lines difficult. Also, many substrates and printed wiring board materials are laminated so the required component of permittivity is normal to the sample face. Transmission-line techniques are useful in PWB applications since the electric field has predominately the right orientation.

The permittivity of a substrate or substrate-thin film composite can be obtained by forming either a stripline from clad substrate (see figure 3.10), microstrip (see figure 3.11), or coplanar fixtures (see figure 3.12), and then either resonating the system or looking at the combined transmission and reflection response. Usually an effective dielectric constant ϵ_{eff} is defined in the numerical modeling which includes the effects of the fields in the

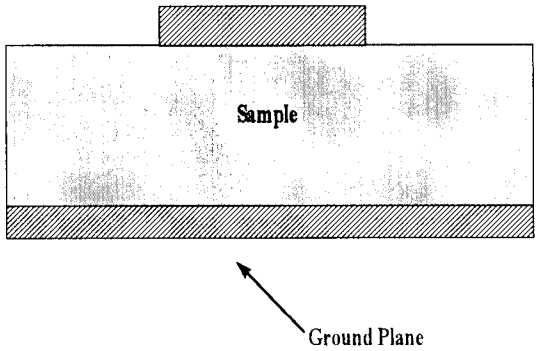

Figure 3.11. Microstrip.

air region surrounding the transmission line. As a result the effective dielectric constant depends on the fields in the specimen and the fringing fields. Theoretical models are usually available that extract the material permittivity from the effective dielectric constant.

Striplines have been used both in resonant and nonresonant modes of operation. A commonly use technique is the stripline-card method. In this technique a stripline is etched into a corner of a large sheet of PWB material. The stripline is then resonated and thereby an estimate of the permittivity is obtained. In another approach the specimen sheet and copper conductors are stacked and then pressure is applied to form a stripline resonator [10].

In stripline we have a quasi-TEM mode and the fixture resonates at frequencies corresponding to integral multiples of one-half wavelength. The real part of the permittivity for stripline is given by

$$\epsilon_r' = \left[\frac{nc}{2f_r(L+\Delta L)}\right]^2, \tag{3.6}$$

where n is the number of half wavelengths, c is speed of light, L is the physical length of transmission line, ΔL is a length extension due to fringing fields, and f_r is the resonance frequency. The loss tangent is calculated from

$$\tan\delta = \frac{1}{Q_{\text{unl}}} + \frac{1}{Q_c}. \tag{3.7}$$

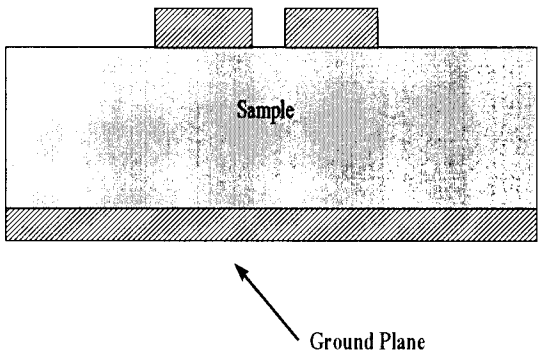

Figure 3.12. Coplanar waveguide fixture.

Q_{unl} is the quality factor not including coupling port losses, but includes losses due to dielectric and metal; Q_c is the quality factor of the coupling probes [90, 94].

A rectangular waveguide measurement technique is shown in figure 3.13 [78]. In this method a specimen is inserted through a slot in the transmission line. The specimen is positioned parallel to the waveguide walls to minimize air-gap depolarization since the electric field is parallel to the sample face. A slight loss of electromagnetic energy occurs due to the presence of the slot.

3.2.10. Coaxial Apertures

Open-ended coaxial lines and waveguides [95,96] have been used for years as nondestructive testing tools. In the open-ended coaxial or waveguide measurement the probe is pressed against a specimen and the reflection coefficient is measured and used to determine the permittivity. Coaxial probes have also been used for elevated temperature measurements of solids and liquids [97]. The technique has been popular and studied extensively. Although nondestructive, the method has definite limitations. The method is sensitive to air gaps since the probe has both E_z and E_ρ electric field components. At low frequencies there is little field interaction with the material. Since the coaxial probe has electric field components in both axial and radial directions, the measurement contains components of

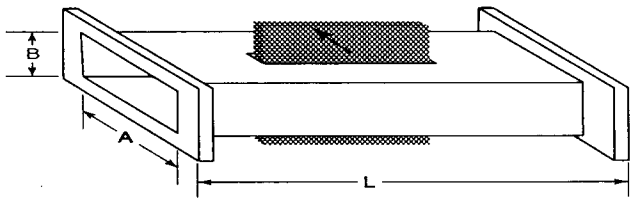

Figure 3.13. Waveguide substrate tester.

both the axial and radial permittivities. The open-ended waveguide technique has the advantage of a tangential electric field at the probe end, thus minimizing the effect of an air-gap. In process control, for example, in thickness testing, a noncontacting probe may be required [97–104]. For this reason it is important to have a model of a coaxial probe which includes *lift-off* [101], or inclusion of an air gap between sample and probe as shown in figure 3.14. The coaxial probe operates at such a frequency where only the fundamental TEM mode propagates in the coaxial line. Evanescent TM_{on} modes are also assumed to exist in the coaxial line near the probe end. In the coaxial line and the material under test, the magnetic field is assumed to be azimuthally symmetric. Therefore only the H_ϕ component needs to be calculated.

Two coaxial probes can be used to form a two-port test device. In this type of fixture

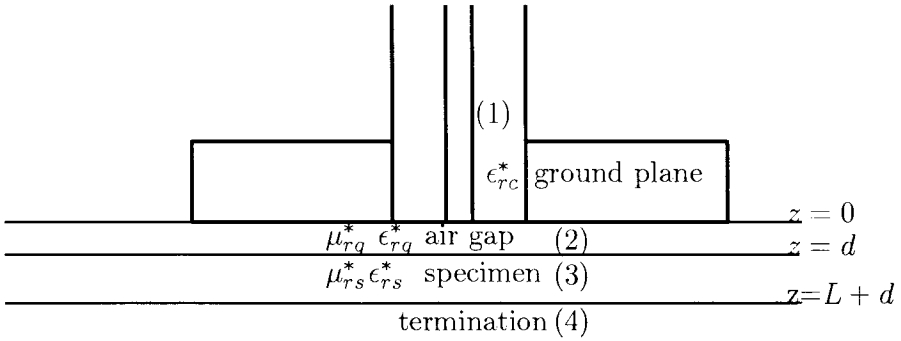

Figure 3.14. The open-ended coaxial probe over a specimen with an air gap between specimen and probe.

a specimen is inserted between the probes and both reflection and transmission data is obtained and inverted for permittivity. The full-mode model is given in reference [34]. The analytical solution follows the same line of reasoning used in the full-mode single coaxial-probe problem. Experimental results indicate that the coaxial probe is useful for broadband material measurements on thin materials as shown in figures 4.1 and 4.2.

Uncertainties in open-ended coaxial measurements include calibration, dimensional, and scattering parameter measurement uncertainties.

The coaxial probe has the advantage of nondestructive testing capability, but the uncertainties are larger than for resonant techniques.

3.2.11. Capacitive Techniques

Capacitance techniques are important at frequencies in the range of 1000 Hz to 100 MHz [105–109]. In these techniques the electric fields are nearly normal to the sample plane. The difficulties with these measurements pertain to air-gap depolarization, electrode polarization, and minimizing the effects of the fringing field. An air gap at the sample-capacitor interface will yield a low value for the real part of the permittivity. The fringe field is usually partially eliminated by measuring the capacitance with and without specimen and subtracting the results. Guards also can protect from fringing fields. At very low frequencies, for conducting materials, electrode polarization is possible. Two-fluid capacitor measurements are frequently used on printed wiring board materials [110]. The technique has the advantage that the material thickness does not enter the calculation. The capacitance is measured in air and then in a fluid, with and without specimen. The

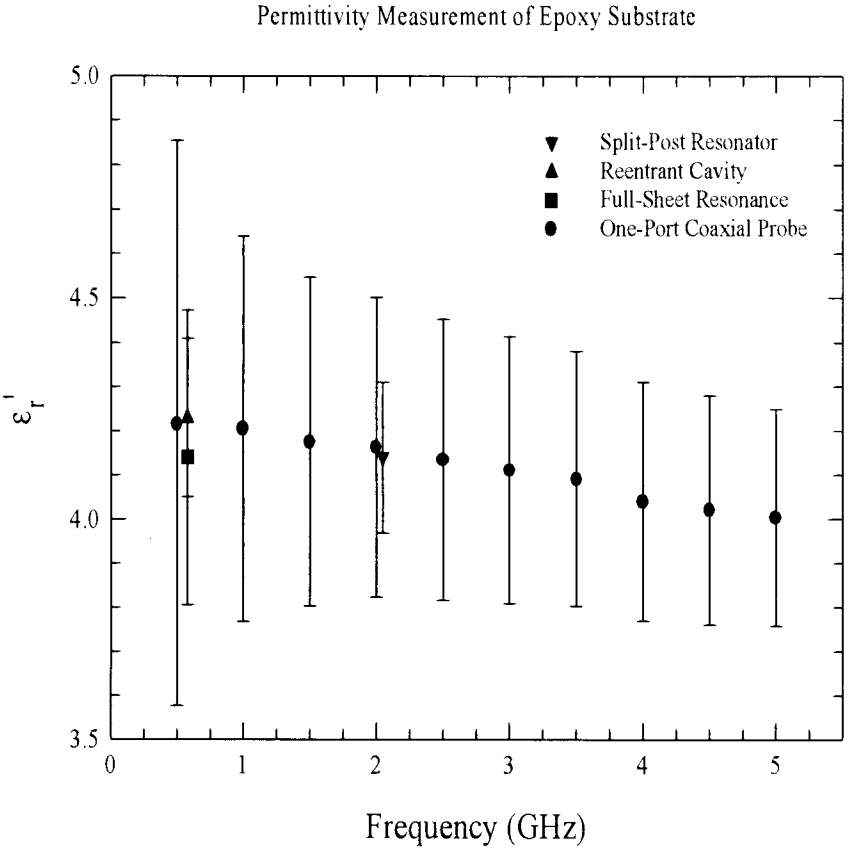

Figure 4.1. Real part of the permittivity from measurements of FR4 material using a coaxial probe compared to measurements made by reentrant cavity, split-post resonator, and full-sheet resonance techniques.

equations are then solved for the permittivity. The fluids used in the method, such as n-heptane, must have very low loss and be well characterized.

4. Measurements

In figures 4.1 and 4.2 coaxial probe measurements are compared to reentrant cavity and full-sheet resonance results.

Measurement results for different materials using a split-dielectric resonator operating at a frequency of approximately 5.6 GHz are shown in tables 4.1 through 4.5 [111]. In table 4.1 three different aluminas from three different manufacturers are given, notice the variation in results. Measurement results for stacked or layered dielectrics are almost in-

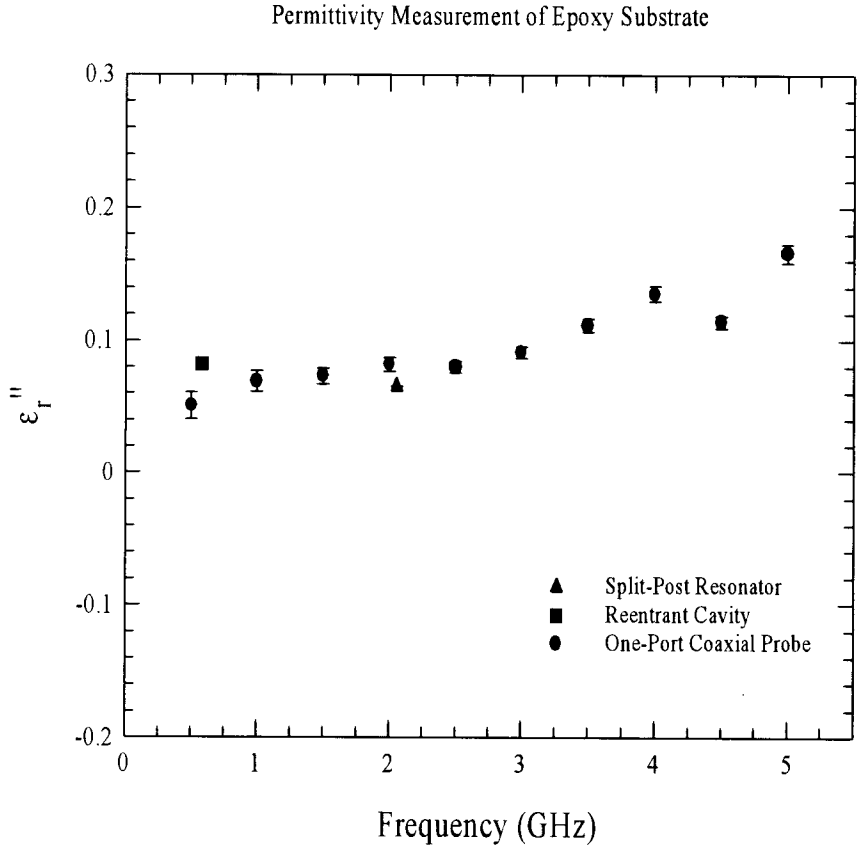

Figure 4.2. Imaginary part of the permittivity from measurements of a FR4 material using a coaxial probe compared to measurements made by reentrant cavity, split-post resonator, and full-sheet resonance techniques.

Table 4.1. Split-dielectric resonator results on low-loss materials [48].

Material	f(MHz)	Q	h(mm)	ϵ_r'	$\tan\delta$ ($\times 10^4$)	$\Delta\epsilon_r'$	$\Delta\tan\delta$ ($\times 10^4$)
Empty	5608.45	9335	0				
Teflon	5587.07	9040	0.620	2.04	2.7	± 0.03	± 1.0
Al_2O_3	5559.31	9639	0.842	9.95	0.4	± 0.03	± 0.5
Al_2O_3	5321.06	9115	0.999	9.75	1.0	± 0.06	± 0.5
Al_2O_3	5406.28	8081	0.740	9.23	2.7	± 0.06	± 0.5

dependent of the number of layers (see table 4.3). Since the field is in the plane of the sample the split dielectric resonator method is not sensitive to the presence of air gaps between stacked films. Since the electric field for the mode of operation has a component only in the plane of the substrate under test, dielectric properties in the plane are determined. Some dielectric substrates may exhibit uniaxial anisotropy. Therefore additional measurements in the direction perpendicular to the substrate are necessary to characterize fully the dielectric properties. Measurement of the component of permittivity normal to the sample plane can be accomplished using the reentrant cavity technique.

In table 4.5 measurements on PWB materials are displayed. A set of measurements using FSR on a number of modes is shown in tables 4.6 and 4.7 and compared with measurements on reentrant cavity [55]. The circle fit procedure is yields a more accurate quality factor and is summarized in [55]. Tables 4.8 to 4.14 report measurements of many materials often used for substrates. The results are presented as data on substrate materials from reference [111]. Figure 4.3 and 4.4 are plots of the permittivity of high-resistivity gallium arsenide as a function of frequency. These measurements were made by X-band cavity. Tables 4.15 through 4.17 and figures 4.5 through 4.12 tabulate measurements of a number of ceramics, plastics, and PWB laminate materials made by other researchers.

Table 4.2. Results from split-dielectric resonators operating unloaded at 10.35 and 12.8 GHz [48].

Material	f(MHz)	Q	h(mm)	ϵ_r'	$\tan\delta$ $(\times 10^4)$	$\Delta\epsilon_r'$	$\Delta\tan\delta$ $(\times 10^4)$
Empty	10375.1	8944	0				
Al_2O_3 (Vistal)	9570.2	9740	0.848	10.03	0.245	± 0.05	± 0.5
Rexolite	10214	7666	0.98	2.53	4.16	± 0.02	± 1
GaAs	9719.5	7134	0.51	12.9	2.75	± 0.02	± 1
Teflon	10304	8709	0.625	2.05	1.61	± 0.03	± 1
Empty	12818	5513	0				
Teflon	12727	5416	0.62	2.034	1.94	± 0.05	± 1
$LaSrAlO_3$	11319	5081	0.50	23.22	1.78	± 0.07	± 1
Al_2O_3	11955	5560	0.70	9.94	1.18	± 0.05	± 0.5

Table 4.3. Split dielectric resonator results on 1 mm thick stacked polymer films of the same material [48].

f(MHz)	Q	h(mm)	ϵ_r'	$\tan\delta$ $(\times 10^4)$	$\Delta\epsilon_r'$	$\Delta\tan\delta$ $(\times 10^4)$	# Films
5608.59	9400	0			empty		
5601.11	8000	0.100	3.19	49	± 0.05	± 4	1
5593.54	6890	0.201	3.20	50	± 0.05	± 3	2
5586.08	6080	0.303	3.20	50	± 0.04	± 2	3
5578.67	5480	0.406	3.20	49	± 0.04	± 1	4
5571.28	4480	0.511	3.19	49	± 0.03	± 1	5
5563.96	4970	0.616	3.18	50	± 0.03	± 1	6

Table 4.4. Measurement results of polymer films from split- dielectric resonators operating unloaded at 1.46 and 2.05 GHz [48].

Material	f(MHz)	Q	h(mm)	ϵ_r'	$\tan\delta$ ($\times 10^4$)	$\Delta\epsilon_r'$	$\Delta\tan\delta$ ($\times 10^4$)
Empty	2055.37	14392	0				
film	2046.00	2020.7	0.96	3.34	324	± 0.02	± 50
Empty	1460.62	16028					
film	1455.27	2487.6	0.96	3.34	323	± 0.02	± 50

Table 4.5. Split dielectric resonator results on printed wiring board materials [48].

Specimen	f (MHz)	Q	h (mm)	ϵ_r'	$\tan\delta$ ($\times 10^4$)	$\Delta\epsilon_r'$	$\Delta\tan\delta$ ($\times 10^4$)
	5608.71	8515				± 0.02	± 4
1	5584.71	2823	0.402	2.77	177	± 0.02	± 4
2	5585.05	2829	0.412	2.71	176	± 0.02	± 4
3	5584.66	2828	0.402	2.78	176	± 0.02	± 4
4	5584.66	2818	0.399	2.79	177	± 0.02	± 4
5	5585.21	2825	0.405	2.73	178	± 0.02	± 4
6	5582.34	5561	0.393	3.28	46.5	± 0.02	± 1
7	5579.97	5413	0.380	3.25	45.9	± 0.02	± 1
8	5579.41	5346	0.380	3.29	46.8	± 0.02	± 1

Table 4.6. FSR measurement on 0.38 mm thick panel. The reentrant cavity result was $\epsilon_r' = 2.45$, $\pm 2\%$ at 440 MHz.

TE Mode	f (MHz)	ϵ_r'	Circle fit FSR	Uncertainty
01	310	2.476	2.488	± 0.007
10	439	2.466	2.478	± 0.009
11	539	2.459	2.449	± 0.017
02	621	2.474	2.478	± 0.011
22	1080	2.462		

Table 4.7. FSR measurement on 1.41 mm thick panel. The reentrant cavity result was $\epsilon'_r = 4.22$, $\pm 1\%$ at 568 MHz. Open-ended coaxial probe yielded $\epsilon'_r = 4.23$ $\pm 5\%$ at 580 MHz.

TE Mode	f (MHz)	ϵ'_r	Circle fit FSR	Uncertainty
01	234	4.059	4.184	± 0.060
10	333	4.092	4.158	± 0.080
11	405	4.001	4.185	± 0.128
02	473	4.084	4.118	± 0.096
12	578	4.019	4.140	± 0.080

Table 4.8. Glass specimens. The standard uncertainties (RSS) are as follows: parallel-plate dielectric resonator: $U_{\epsilon'} = 0.5\%$, $U_{\tan\delta} = 2 \times 10^{-5}$, split-cavity: $U_{\epsilon'} = 1\%$, $U_{\tan\delta} = 1 \times 10^{-4}$, TE_{01} cavity resonator: $U_{\epsilon'} = 1\%$, $U_{\tan\delta} = 1 \times 10^{-4}$, Fabry-Perot resonator: $_{\epsilon'} = \pm 2\%$, $U_{\tan\delta} = 2 \times 10^{-4}$, reentrant cavity: $_{\epsilon'} = \pm 1\%$, $U_{\tan\delta} = 2 \times 10^{-4}$.

Material	Value	Parallel plate	Split cavity	60 mm TE_{01}	Split post	Reentrant
Corning	f(GHz)	5.07	8.85	9.64	2.03	
7980	ϵ'	3.84	3.827	3.84	3.84	
34604	$\tan\delta$	6.85×10^{-5}	11.9×10^{-5}	1.40×10^{-4}	4.40×10^{-5}	
Corning	f(GHz)	5.07	8.82	9.63	2.03	
7980	ϵ'	3.844	3.822	3.843	3.838	
34605	$\tan_\delta$	6.8×10^{-5}	11.7×10^{-5}	1.4×10^{-4}	3.1×10^{-5}	
Corning	f(GHz)	5.26	8.86	9.64	2.03	
7980	ϵ'	3.844	3.825	3.826	3.84	
34606	$\tan\delta$	6.90×10^{-5}	1.80×10^{-4}	1.5×10^{-4}	4.9×10^{-5}	
Corning	f(GHz)	4.89	8.86	9.64	2.03	
7940	ϵ'	3.847	3.825	3.826	3.839	
44608	$\tan\delta$	6.83×10^{-5}	11.6×10^{-5}	1.4×10^{-4}	3.6×10^{-5}	
Corning	f(GHz)	9				1
H. Bussey	ϵ'	6.20				6.21
1723 (1959)	$\tan\delta$	5.36×10^{-3}				3.2×10^{-3}

Table 4.9. Plastic specimens of polytetrafluoroethylene (PTFE), cross-linked polystyrene (CPS), fluoroethylenepropylene (FEP), polymethylmethacrylate (PMMA), and nylon. The standard uncertainties (RSS) are as follows: parallel-plate dielectric resonator: $U_{\epsilon'} = 0.5\%$, $U_{\tan\delta} = 2 \times 10^{-5}$, TE_{01} cavity resonator: $U_{\epsilon'} = 1\%$, $U_{\tan\delta} = 1 \times 10^{-4}$, reentrant cavity: $U_{\epsilon'} = 2\%$, $U_{\tan\delta} = 2 \times 10^{-4}$.

Material	Value	Parallel plate	60 mm TE_{01}	Reentrant cavity
FEP	f (GHz)	6.59	9.837	
	ϵ'	2.064	2.025	
	$\tan\delta$	7.04×10^{-4}	3.12×10^{-4}	
PTFE	f (GHz)	9.93	9.816	1.082
	ϵ'	2.05	2.055	2.06
	$\tan\delta$	2.0×10^{-4}	2.1×10^{-4}	$3. \times 10^{-4}$
CPS	f (GHz)	5.7	9.982	1.032
	ϵ'	2.542	2.533	2.56
	$\tan\delta$	5.1×10^{-4}	4.2×10^{-4}	7×10^{-4}
Nylon	f (GHz)	4.75	9.742	
	ϵ'	3.08	3.01	
	$\tan\delta$	8.4×10^{-3}	7.1×10^{-3}	
PMMA	f (GHz)	5.721	9.813	
	ϵ'	2.634	2.626	
	$\tan\delta$	7.2×10^{-3}	4.4×10^{-3}	

Table 4.10. Cubic single crystals. The standard uncertainties (RSS) are as follows: parallel-plate dielectric resonator: $U_{\epsilon'} = 0.5\%$, $U_{\tan\delta} = 2\times10^{-5}$, whispering gallery Mode resonator: $U_{\epsilon'} = 0.1\%$, $U_{\tan\delta} = 2 \times 10^{-5}$. Anisotropic materials were measured either by two dominant modes (TE_{0111} and HE_{111}) using the parallel plate rod resonator or two families of whispering gallery modes.

Material	Value	Parallel Plate
$LaAlO_3$	freq. (GHz)	18.38
(cubic)	ϵ'	23.99
	$\tan\delta$	1.0×10^{-5}
$NdGaO_3$	f (GHz)	18.49
(cubic)	ϵ'	21.82
	$\tan\delta$	1.07×10^{-4}
Zirconia	f (GHz)	4.30
(cubic)	ϵ'	27.8
	$\tan\delta$	3.28×10^{-3}
GGG	f (GHz)	15.7
(cubic)	ϵ'	12.43
	$\tan\delta$	2.64×10^{-3}
$SrTiO_3$	f (GHz)	7.20
(cubic)	ϵ'	310
	$\tan\delta$	4.01×10^{-4}
MgO	f (GHz)	17.46
(cubic)	ϵ'	9.70
	$\tan\delta$	2.5×10^{-6}

Table 4.11. Noncubic single crystals. The standard uncertainties (RSS) are as follows: parallel-plate dielectric resonator: $U_{\epsilon'} = 0.5\%$, $U_{\tan\delta} = 2 \times 10^{-5}$, whispering gallery Mode resonator: $U_{\epsilon'} = 0.1\%$, $U_{\tan\delta} = 2 \times 10^{-5}$. Anisotropic materials were measured either by two dominant modes (TE_{0111} and HE_{111}) using the parallel plate rod resonator or two families of whispering gallery modes.

Material	Value	Parallel plate	Whispering gallery
Al_2O_3	f (GHz)	10.0	12.4
$\parallel$ c-axis	ϵ'	11.58	11.58
(sapphire)	$\tan\delta$	2×10^{-5}	$5. \times 10^{-6}$
Al_2O_3	f (GHz)		12.4
$\perp$ c-axis	ϵ'		9.40
(sapphire)	$\tan\delta$	2×10^{-5}	$7. \times 10^{-6}$
$LiNbO_3$	f (GHz)	10.19	
$\parallel$ c-axis	ϵ'	32.97	
	$\tan\delta$	$8. \times 10^{-5}$	
$LiNbO_3$	f (GHz)	11.56	
$\perp$ c-axis	ϵ'	42.34	
	$\tan\delta$	8.4×10^{-5}	
Quartz	f (GHz)	7.75	
$\perp$ c-axis	ϵ'	4.59	
	$\tan\delta$	1.5×10^{-5}	
Quartz	f (GHz)	9.03	
$\parallel$ c-axis	ϵ'	4.443	
	$\tan\delta$	1.3×10^{-5}	
TiO_2	f (GHz)		4.2
$\parallel$ c-axis	ϵ'		163.7
	$\tan\delta$		1×10^{-4}
TiO_2	f (GHz)		4.2
$\perp$ c-axis	ϵ'		85.6
	$\tan\delta$		8×10^{-5}

Table 4.12. Low-medium dielectric constant ceramic specimens. The standard uncertainties (RSS) are as follows: parallel-plate dielectric resonator: $U_{\epsilon'} = 0.5\%$, $U_{\tan\delta} = 2 \times 10^{-5}$, TE_{01} cavity resonator: $U_{\epsilon'} = 1\%$, $U_{\tan\delta} = 1 \times 10^{-4}$, whispering gallery mode resonator: $U_{\epsilon'} = 0.1\%$, $U_{\tan\delta} = \pm 2 \times 10^{-5}$.

Material	Value	Parallel Plate	60 mm Cavity	Whispering Gallery
Ceramic	f (GHz)	3.675	9.76	
4	ϵ'	4.704	4.686	
	$\tan\delta$	6.8×10^{-4}	5.80×10^{-4}	
Ceramic	f (GHz)	3.17	9.74	
6	ϵ'	6.592	6.592	
	$\tan\delta$	4.58×10^{-4}	5.30×10^{-4}	
Ceramic	f (GHz)	2.713	9.74	
9	ϵ'	9.808	9.73	
	$\tan\delta$	2.55×10^{-4}	2.50×10^{-4}	
Alumina	f (GHz)	3.27	9.53	9.528
(1986)	ϵ'	10.04	10.02	9.98
	$\tan\delta$	3.9×10^{-5}	3.38×10^{-5}	3.2×10^{-5}
Alumina	f (GHz)	9.00		
(1996)	ϵ'	9.992		
	$\tan\delta$	1.30×10^{-3}		

Table 4.13. High-dielectric constant ceramic specimens. The standard uncertainties (RSS) are as follows: parallel-plate dielectric resonator: $U_{\epsilon'} = 0.5\%$, $U_{\tan\delta} = 2\times10^{-5}$, TE_{01} cavity resonator: $U_{\epsilon'} = 1\%$, $U_{\tan\delta} = 1 \times 10^{-4}$, whispering gallery mode resonator: $U_{\epsilon'} = 0.1\%$, $U_{\tan\delta} = \pm2 \times 10^{-5}$

Material	Value	Parallel plate	60 mm cavity	Whispering gallery
Ceramic	f (GHz)	1.987	9.72	9.577
13	ϵ'	13.51	13.55	13.54
	$\tan\delta$	1.07×10^{-4}	1.10×10^{-4}	1.01×10^{-4}
Ceramic	f (GHz)	1.834	9.71	9.692
16	ϵ'	16.60	16.64	16.66
	$\tan\delta$	2.43×10^{-5}	0.4×10^{-4}	5.70×10^{-5}
Ceramic	f (GHz)	1,617	9.70	
20	ϵ'	20.77	20.80	
	$\tan\delta$	8.4×10^{-5}	2.00×10^{-4}	
Ceramic	f (GHz)	1.328	9.44	6.023
31	ϵ'	30.96	31.03	30.99
	$\tan\delta$	2.4×10^{-5}	5.0×10^{-5}	4.9×10^{-5}
Ceramic	f (GHz)	1.200	9.46	5.460
35	ϵ'	35.15	35.19	35.14
	$\tan\delta$	4.8×10^{-5}	1.6×10^{-4}	1.18×10^{-4}
Ceramic	f (GHz)	1.116	9.46	4.812
36	ϵ'	36.55	36.56	36.55
	$\tan\delta$	3.3×10^{-5}	1.2×10^{-4}	8.8×10^{-5}
Ceramic	f (GHz)	1.109	9.73	
38	ϵ'	38.65	38.77	
	$\tan\delta$	5.8×10^{-5}	3.0×10^{-4}	
Ceramic	f (GHz)	2.83		
78	ϵ'	78.29		
	$\tan\delta$	3.1×10^{-4}		
Ceramic	f (GHz)	0.855	9.44	4.448
79	ϵ'	79.27	79.29	79.11
	$\tan\delta$	1.63×10^{-4}	7.8×10^{-4}	4.40×10^{-4}

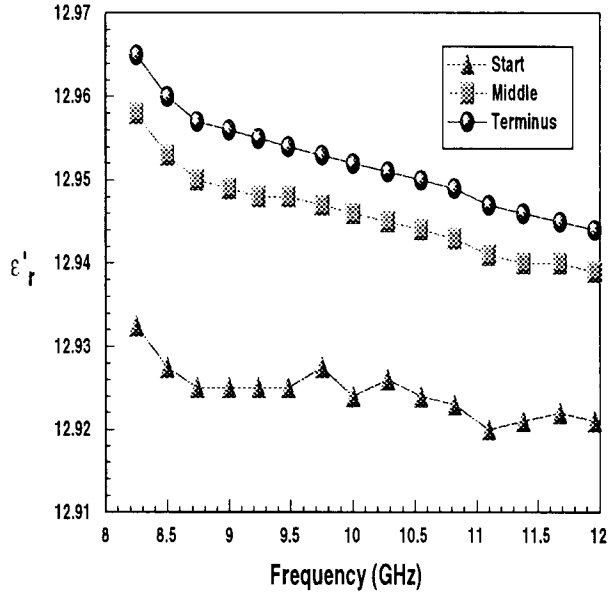

Figure 4.3. Measurement of the real part of the permittivity of gallium arsenide using an X-band cavity [112]. Start, middle, and terminus refer to different specimens taken from the same boule.

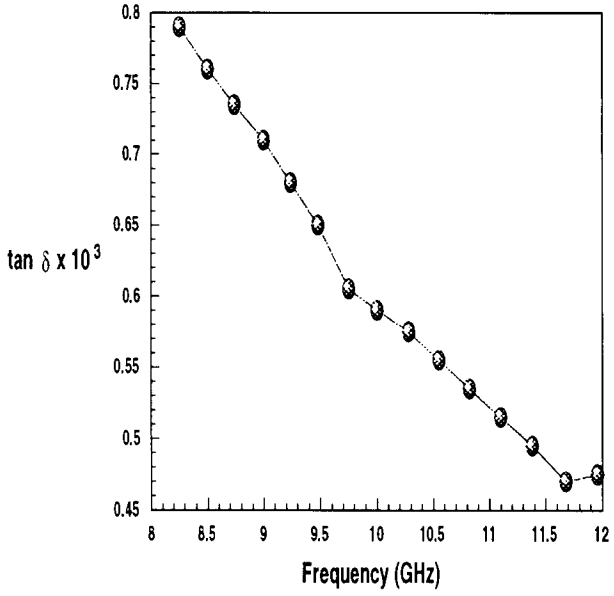

Figure 4.4. Measurement of the loss tangent of gallium arsenide using an X-band cavity [112].

Table 4.14. 1964 round-robin measurements compared with current measurements. The round-robin results from 1964 are given below [113,114]. The standard uncertainties (RSS) are as follows: parallel-plate dielectric resonator: $U_{\epsilon'} = 0.5\%$, $U_{\tan\delta} = 2\times10^{-4}$, TE_{01} cavity resonator: $U_{\epsilon'} = 1\%$, $U_{\tan\delta} = 1 \times 10^{-4}$.

Material	Value	NBS(1964)	Parallel Plate	TE_{01} (50 mm)	TE_{01} (60 mm)
1723 Glass	f (GHz)	9		10	
(1964 RR)	ϵ'	6.20		6.26	
	$\tan\delta$	5.3×10^{-3}		4.8×10^{-3}	
1723 Glass	f (GHz)	9		9.58	10
(1972 RR)	ϵ'	6.155		6.16	6.146
	$\tan\delta$	4.7×10^{-3}		4.9×10^{-3}	4.7×10^{-3}
7940 Glass	f (GHz)	9	9	10	9.82
(1972 RR)	ϵ'	3.826	3.822	3.828	3.829
	$\tan\delta$	1.2×10^{-4}	1.4×10^{-4}	1.03×10^{-4}	1.2×10^{-4}

Table 24. Additional dielectric measurements on ceramics and crystals.

Material	Crystal	f (GHz)	ϵ_r'	$\tan\delta$
Aluminum nitride [115]	No	8.5	8.5	0.0030
Barium borate	Yes	0.001	4.6	0.0005
Beryllium oxide [115]	Yes	8.5	6.86	0.0003
Boron nitride [115]	No	5.0	4.30	0.0002
Calcium carbonate [115]	Yes	0.0001	8.5	0.0004
Calcium fluoride [115]	Yes	1	6.3	0.0006
Germanium[115]	Yes	10	16.6	
Lithium niobate[115]	Yes	10	29	
Neodymium gallate [115]	Yes	10	20	0.0030
Nickel oxide[115]	No	1	7.5	0.0001
Silicon nitride [115]	No	8.5	5.5	0.0036
Potassium bromide[115]	Yes	10	4.9	
Silicon [115]	Yes	14	12	0.0090
Silicon carbide[24]	No	10	9.7	0.0010
Sodium chloride[115]	Yes	0.001	5.7	0.0001
Strontium lanthanum aluminate[115]	Yes	10	17	0.0008
Strontium lanthanum gallate[115]	Yes	10	22	0.0001
Topaz [115]	Yes	0.01	6.5	0.0001
Yttrium iron garnet [115]	Yes	10	14.9	0.0001
Yttrium oxide [115]	No	0.001	11.3	0.0006
Zinc oxide [115]	No	0.01	8.3	0.0300

Table 4.16. Additional dielectric measurements made on plastics.

Material	f (GHz)	ϵ_r'	$\tan\delta$
PMMA [115]	3.0	2.61	0.0057
Nylon [115]	3.0	2.84	0.0117
Polyethylene [115]	3.0	2.26	0.0003
Styrofoam [115]	3.0	1.03	0.0002
Polyimide [23]	0.001	3.50	0.0003
Polysulfone [116]	1.0	3.02	0.0090
Polyolefin [116]	1.0	2.75	0.0200

Table 4.17. Dielectric measurements of PWB composites.

Material	range of ϵ_r'
FR-4 [10]	4.2-5.0
FR-5 (high temp) [10]	4.3-4.6
BT/epoxy [10]	4.0-4.2
Cyanate ester [10]	3.5-3.7
Arimid/epoxy [10]	3.7-3.9
Polyimide/glass [10]	3.9-4.2
Polyimide/quartz [10]	3.4-3.5

5. Elevated Temperature Measurements

Many substrate and PWB materials vary with temperature. In this section we will describe a system for making elevated temperature measurements; we also present permittivity measurements as a function of temperature for a number of substrate materials. We use a $TE_{01\delta}$ dielectric resonator as shown in figure 5.1 for these measurements. The specimen is supported by a low-loss dielectric rod in order to minimize wall losses. The temperature system as shown in figure 5.2 is an environmental chamber that operates from -80 ^{o}C to 300 ^{o}C. We use cavities, transmission lines, and reentrant cavities in the chamber. The chamber has access holes on the sides for insertion of coaxial feeds for the cavities or transmission lines. The chamber can also be purged with nitrogen gas to reduce oxidation and water vapor.

Measurements of some common low dielectric constant materials are given in figures 5.3 to 5.8.

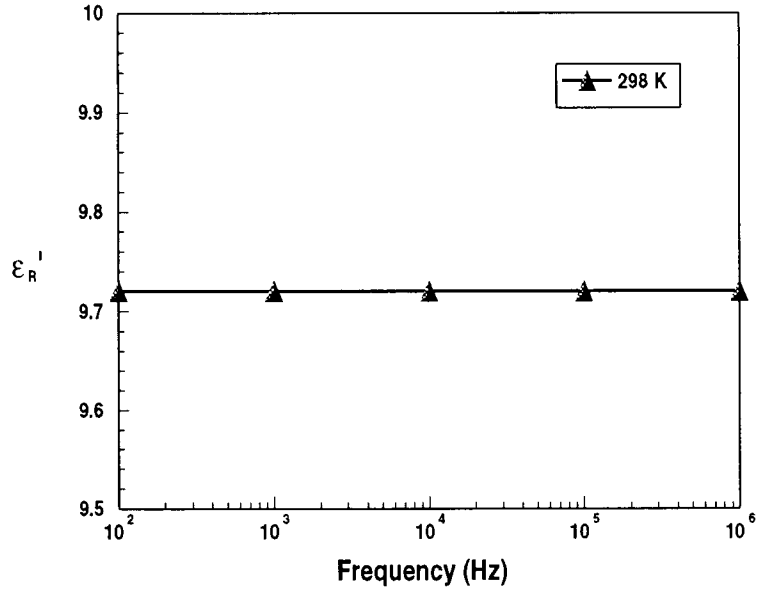

Figure 4.5. Measurements on the real part of the permittivity for MgO [115].

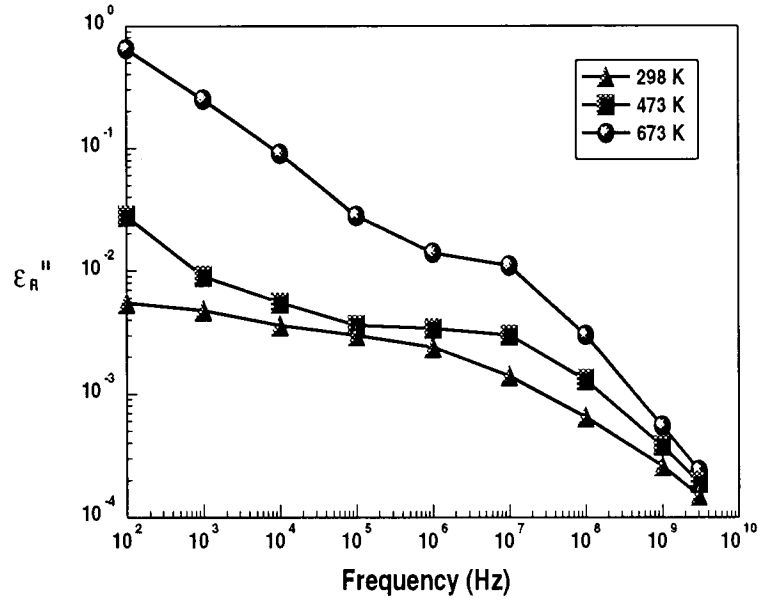

Figure 4.6. Measurements on the loss part for MgO [115].

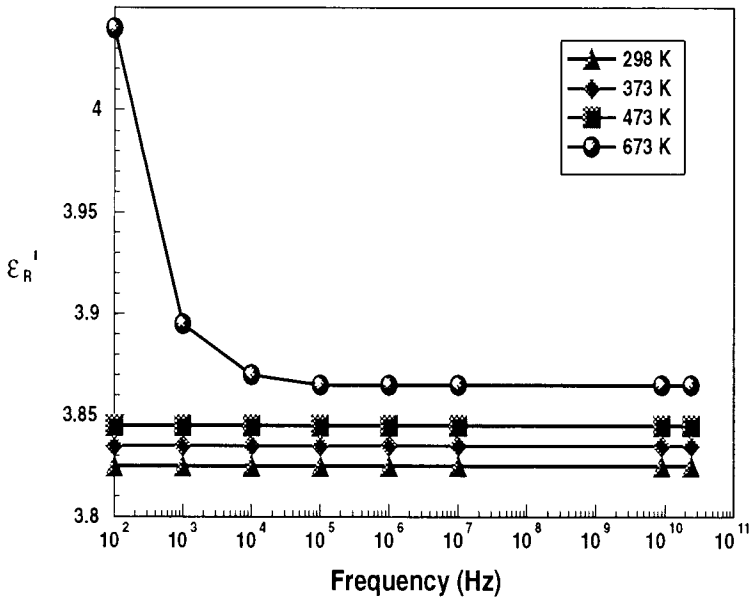

Figure 4.7. Measurements on the real part of the permittivity for SiO_2 as a function of temperature [115].

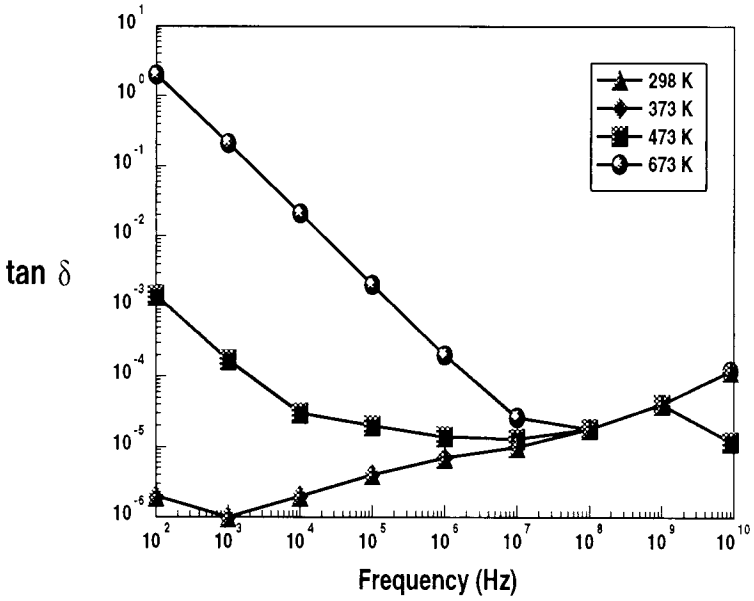

Figure 4.8. Measurements on the loss part for SiO_2 as a function of temperature [115].

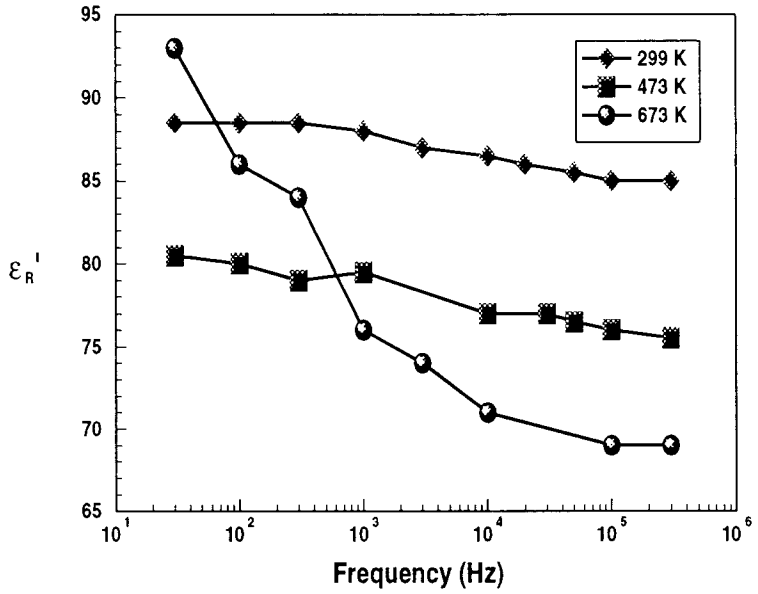

Figure 4.9. Measurements on the real part of the permittivity for rutile with electric field perpendicular to axis as a function of temperature [115].

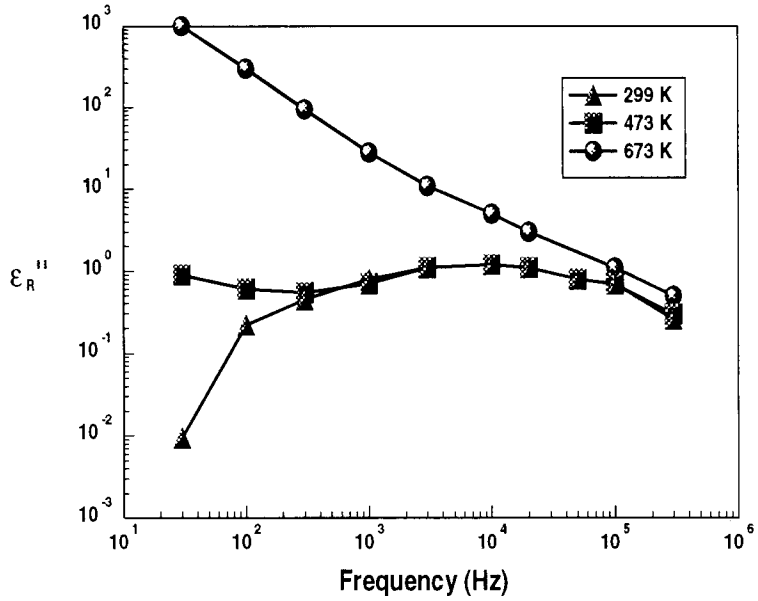

Figure 4.10. Measurements on the loss part for rutile with electric field perpendicular to axis as a function of temperature [115].

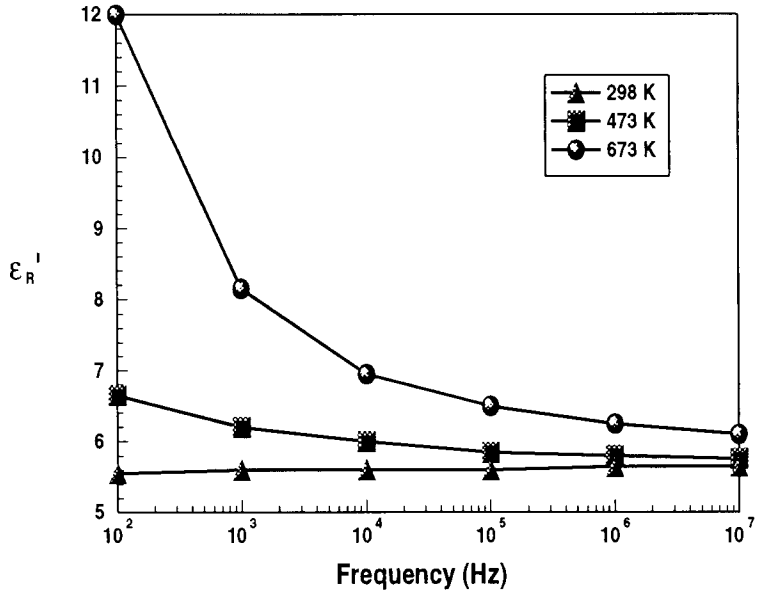

Figure 4.11. Measurements on the real part of the permittivity for silicon nitride as a function of temperature [115].

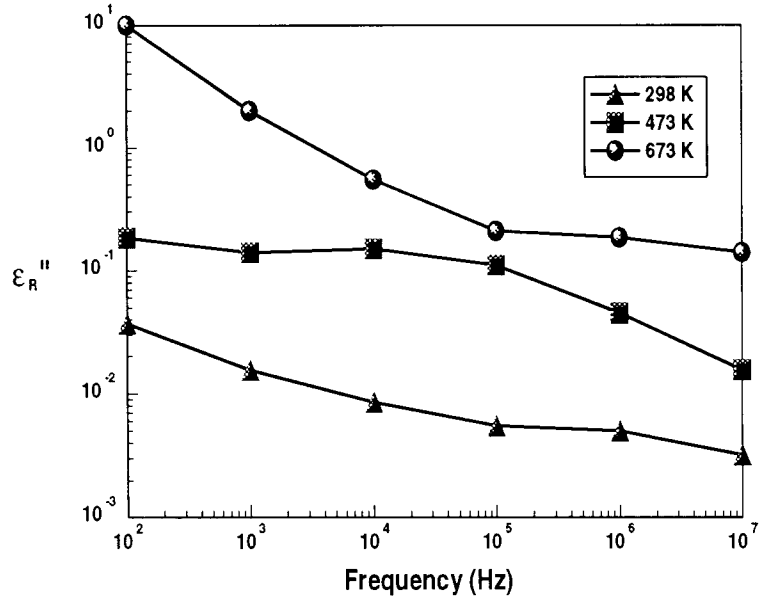

Figure 4.12. Measurements on the loss part for silicon nitride as a function of temperature [115].

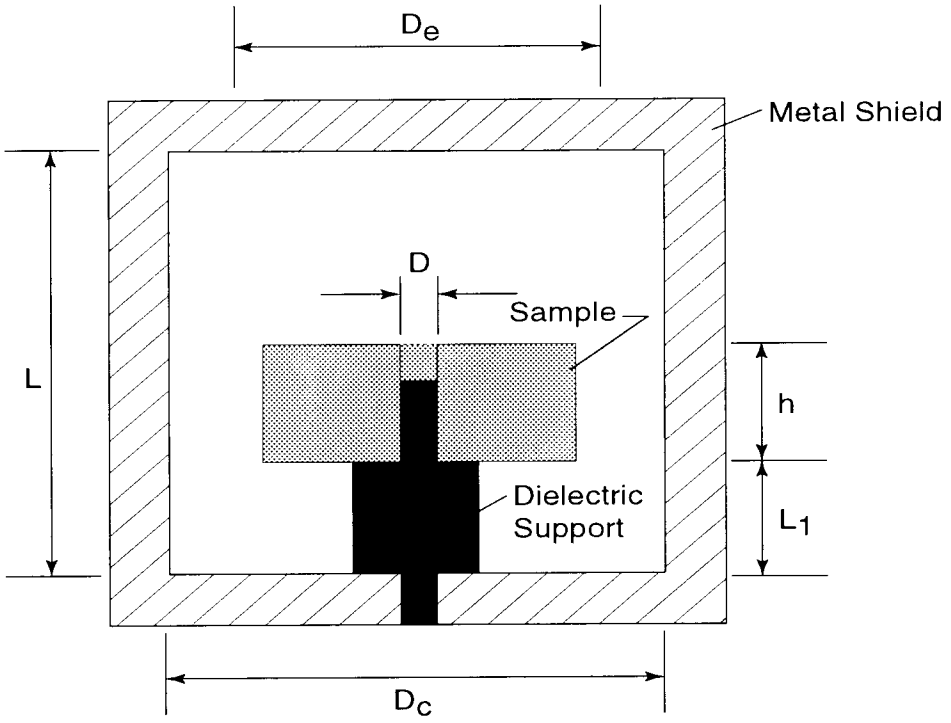

Figure 5.1. $TE_{01\delta}$ resonator for elevated temperature measurements.

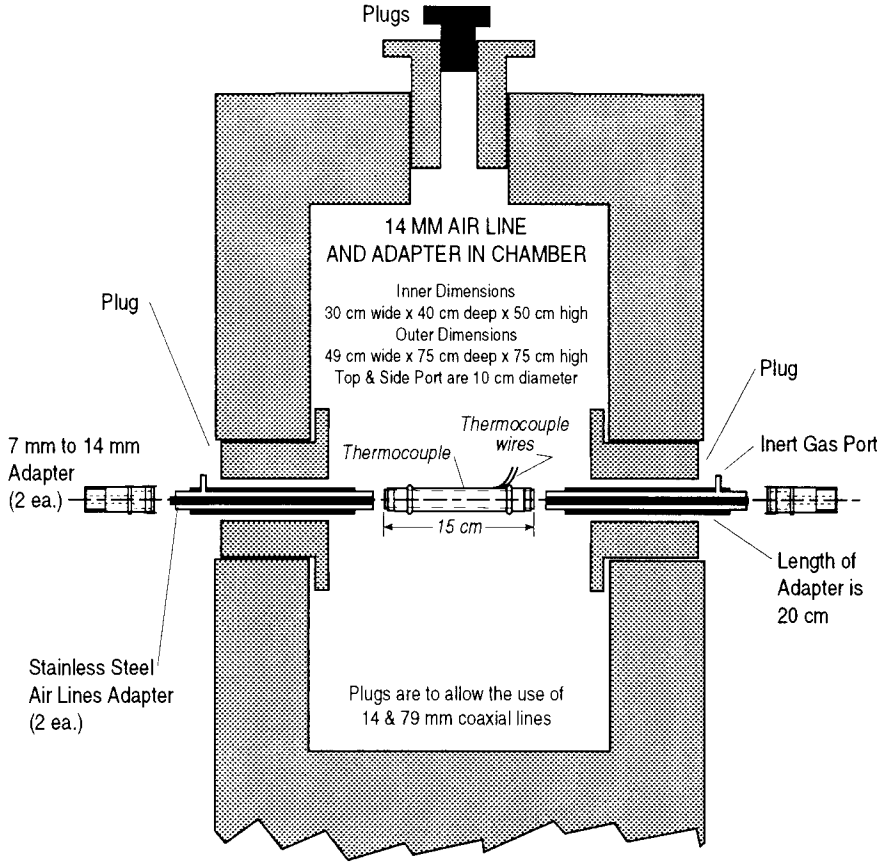

Figure 5.2. Environmental chamber for elevated temperature measurements.

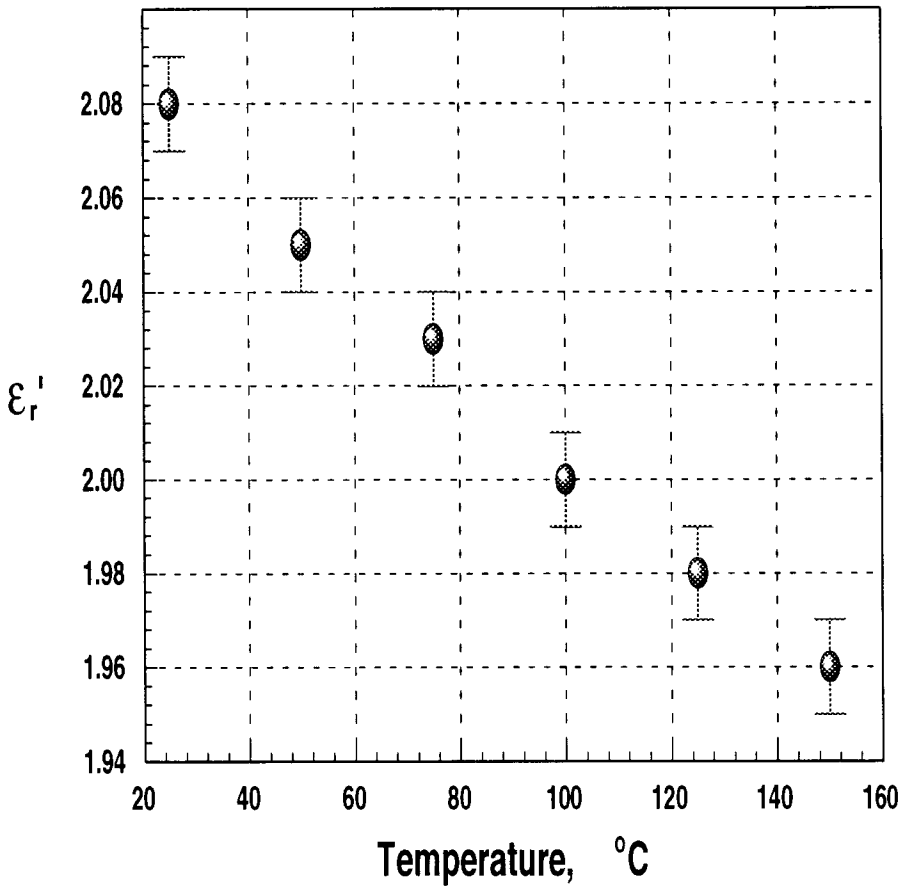

Figure 5.3. Real part of the permittivity of Teflon as a function of temperature.

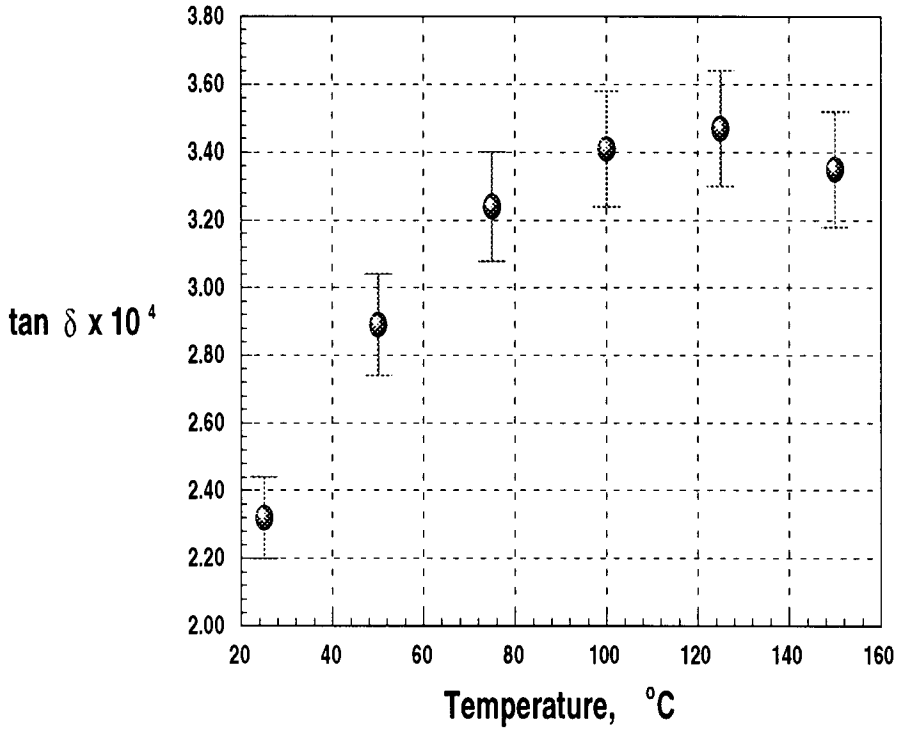

Figure 5.4. Loss tangent of Teflon as a function of temperature at 10 GHz.

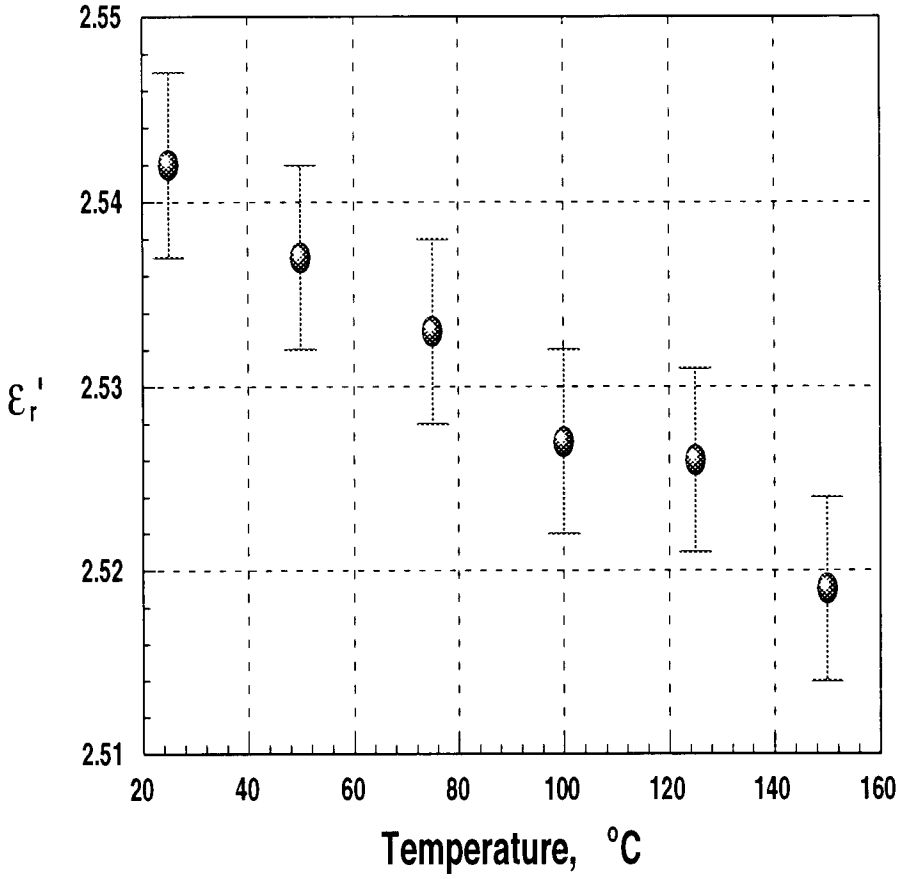

Figure 5.5. Real part of the permittivity of Rexolite as a function of temperature at 10 GHz.

6. Conclusion

Each technique we have reviewed has a niche in the frequency band, field behavior, and loss characteristics of printed wiring board and substrate materials. One technique alone is not sufficient to characterize materials over all of the necessary parameters. Measurements of substrate materials present a metrological challenge because of uncertainty in thickness and anisotropy. Typical PWB materials have a thickness of between 0.2 to 3 mm. Large uncertainties of thin materials are caused by large thickness uncertainties. Measurement with this type of field orientation can suffer from the effects of air gap.

The reentrant cavity, stripline, and full-sheet resonance techniques are useful for mea-

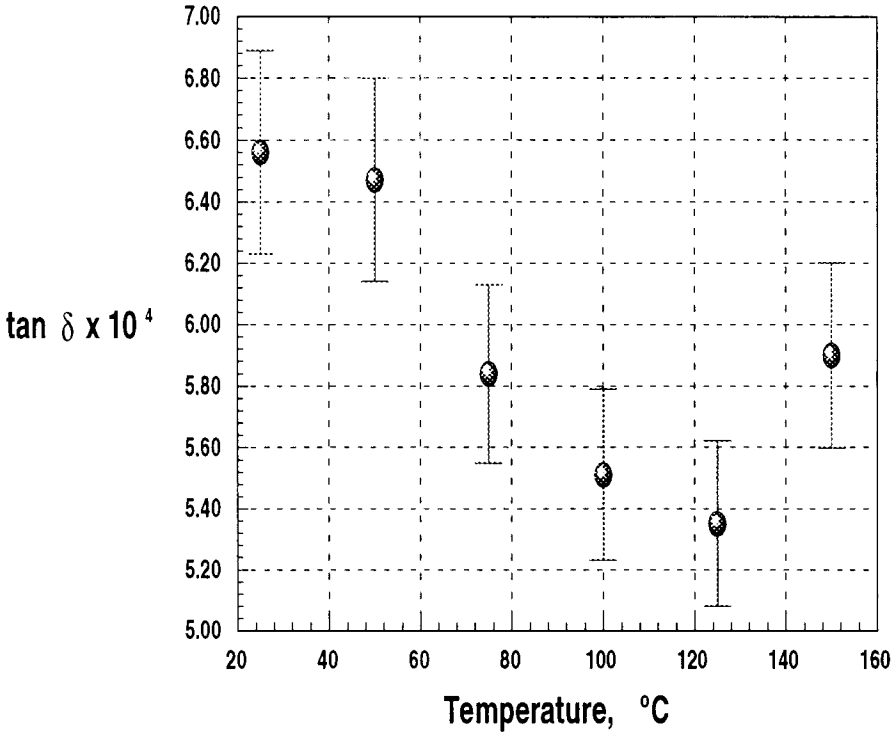

Figure 5.6. Loss tangent of Rexolite as a function of temperature.

Table 5.1. Dielectric measurement categories compared.

Technique	Field	Advantages	Disadvantages	$\Delta\epsilon_r'$	$\Delta \tan \delta_r$
Full-sheet resonance	TE_{10}	ϵ_r'	Poor ϵ_r''	± 2	
Transmission-line	TEM,TE_{10}	Broadband	Machining of specimen	$\pm 5\%$	± 0.01
Capacitor	Capacitor	Normal E-field	Air gap	$\pm 1\%$	$\pm 10^{-4}$
Cavity	TE_{01}	Very Accurate	Narrow band	$\pm 0.2\%$	$\pm 5 \times 10^{-5}$
Cavity	TM_{0m}	ϵ_{rz}'	Air gap	$\pm 0.5\%$	$\pm 5 \times 10^{-4}$
Dielectric resonator	TE_{01}	Very Accurate	Low-loss region	± 0.2	$\pm 5 \times 10^{-5}$
Open-ended probe	TEM, TM_{01}	Nondestructive	Contact problem	$\pm 10\%$	± 0.02
Fabry-Perot	Quasi-TEM	High frequency	Low-loss materials	$\pm 2\%$	± 0.0005

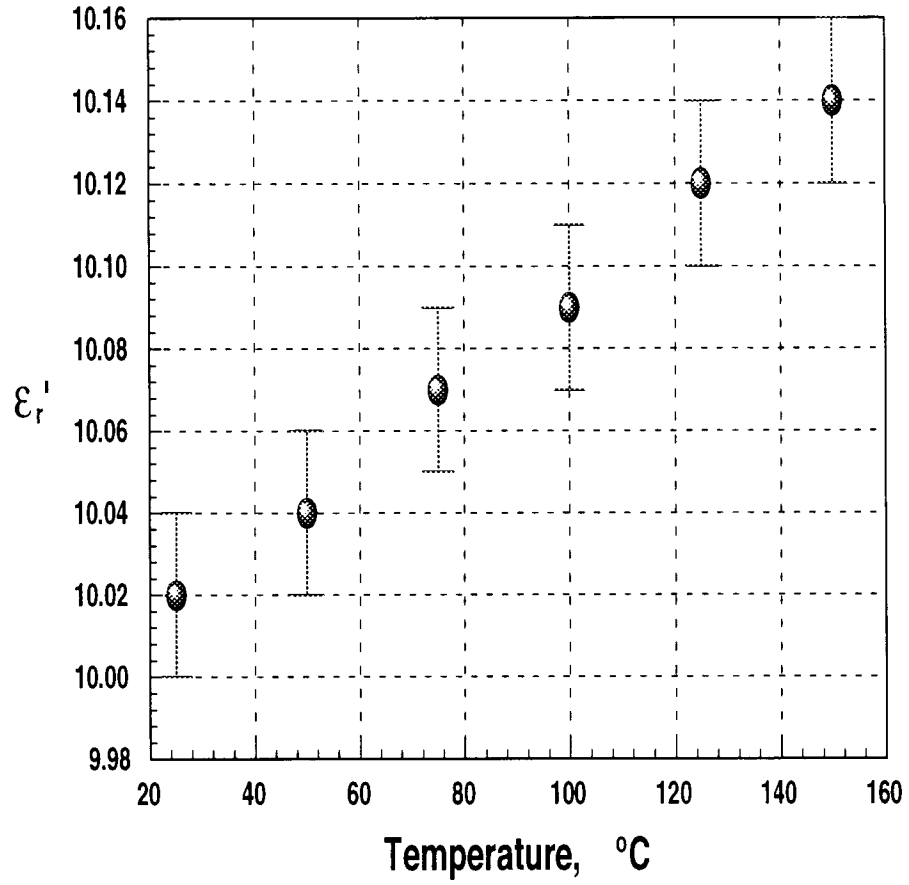

Figure 5.7. Real part of the permittivity of alumina as a function of temperature at 10 GHz.

Table 5.2. Magnetic measurement methods compared.

Technique	Field	Advantages	Disadvantages	$\Delta\epsilon_r'$	$\Delta \tan\delta_r$
Transmission-line	TEM,TE_{10}	Broadband	Machining of specimen	$\pm 2\%$	± 0.01
Cavity	TE_{011}	Very accurate	Low loss	$\pm 0.5\%$	$\pm 5 \times 10^{-4}$
Cavity	TM_{110}	μ_{rz}'	Low loss	$\pm 0.5\%$	$\pm 5 \times 10^{-4}$
Dielectric resonator	TE_{011}	Very accurate	Low loss	$\pm 0.5\%$	$\pm 5 \times 10^{-4}$
Whispering-gallery	Hybrid	Very accurate	High frequency	± 1	$\pm 5 \times 10^{-6}$
Courtney	TE_{01}	Very accurate	Use sleeves	± 1	$\pm 5 \times 10^{-5}$

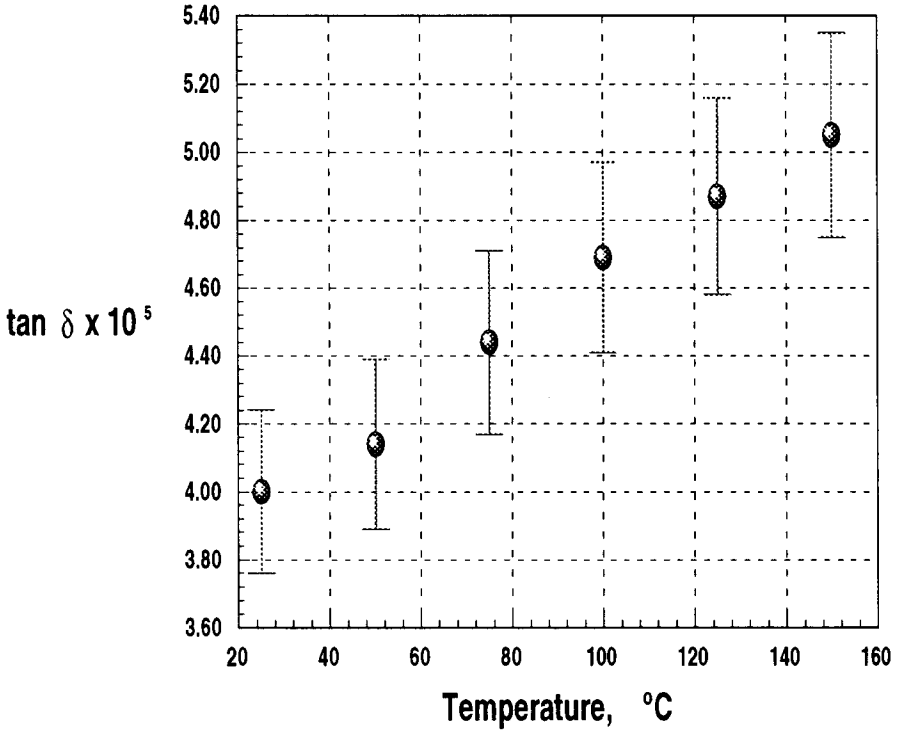

Figure 5.8. Loss tangent of alumina as a function of temperature.

surement of the component of permittivity normal to the sample face. The reentrant cavity technique has difficulty with specimens thinner than 0.5 mm; however, it yields a good measurement of loss. TM_{0m} cavities yield a measurement with the electric field normal to the specimen face. These cavities can measure over a frequency band of 1 to 10 GHz by using higher modes. The stripline technique has the advantage of easily accommodating PWB materials. It gives reasonable estimates for the real part of the permittivity and borderline estimates for the imaginary part of the permittivity. Many of the important features of the most important measurement techniques are summarized in tables 5.1 and 5.2. The split-cavity and split-post resonators are useful for obtaining in-plane permittivity and loss. Whispering-gallery modes are very sensitive to loss. Fabry-Perot resonators are useful at high frequencies. The coaxial probe techniques are useful in obtaining permittivity of isotropic materials with medium accuracy.

The full characterization of thin, anisotropic materials generally requires two techniques, one for the component of permittivity normal to specimen face and one for in-plane permittivity. However, the loss measurement is not affected as much as the real part of the permittivity by anisotropy and a single measurement often suffices. Therefore for the normal-field measurement, resonant transmission-line methods can be used. However the loss could be obtained by more accurate in-plane techniques such as TE_{01} resonators.

Magnetic substrate measurement requires a strong magnetic field. Magnetic materials can be measured by a split-post magnetic resonator, TM_{110} [43] or TE_{011} cavities, whispering-gallery modes, or TE_{011} cavities or dielectric resonators (see table 5.2).

We would like to thank J. Krupka and R. Geyer for measurement assistance. Also Brad Givot for reviewing the report.

7. References

[1] Bahl, I.; Ely, K. Modern microwave substrate materials. Microwave J. (State of the Art Reference) 33: 131–146; 1990.

[2] Chang, C. S.; Agrawal, A. P. Fine line thin dielectric circuit board characterization. Proc. 44th Electronic Components and Technology Conf.; 564–569. Comp., Hybrids, Mfg. Technol. Soc.; 1994.

[3] Chang, C. S. Resistive signal line wiring net designs in multichip modules. IEEE Trans. Comp., Hybrids, Mfg. Technol. 16: 909–918; 1993 December.

[4] Westphal, W. P. Techniques of measuring the permittivity and permeability of liquids and solids the frequency range 3 c/s to 50 kMc/s. MIT XXXVI; 1950.

[5] Baker-Jarvis, J.; Janezic, M. D.; Grosvenor, J. H.; Geyer, R. G. Transmission/reflection and short-circuit line methods for measuring permittivity and permeability. Natl. Inst. Stand. Technol. Tech. Note 1355; revised 1994; 1994.

[6] Hippel, V. Dielectric Materials and Applications. Cambridge, MA: M.I.T. Press; 1954.

[7] Nicolson, A. M.; Ross, G. F. Measurement of the intrinsic properties of materials by time domain techniques. IEEE Trans. Instrum. Meas. IM-19: 377–382; 1968 November.

[8] Bussey, H. E.; Gray, J. E. Measurement and standardization of dielectric samples. IRE Trans. Inst. I-11(3): 162–165; 1962.

[9] Baker-Jarvis, J.; Janezic, M. D. Open-ended coaxial probes for nondestructive testing of substrates and circuit boards. Iskander, M., Ed., Proc. Microwave Processing of Materials IV; 347; 215–220. MRS; 1994.

[10] Fjelstad, J. Printed circuit technology materials and processes. The Institute for Interconnecting and Packaging Electronic Circuits 1; 1995.

[11] Laverghetta, T. S. Microwave materials and fabrication techniques. New York: Artech House; 1990.

[12] Ibarra, A.; Gonzalez, M.; Vila, R. Dielectric properties of some organic RF-substrates. Micro. Eng. Europe 1: 25–34; 1998 May.

[13] Traut, G. R. Clad laminates of PTFE composites for microwave antennas. Microwave J. 23: 47–53; 1980 November.

[14] Sasaki, A.; Shimada, Y. Electrical design technology for low dielectric constant multilayer ceramic substrate. IEEE Trans. Comp., Hybrids, Mfg. Technol. 15: 56–62; 1992 February.

[15] Takahashi, A.; Nagai, A.; Mukoh, A.; Wajima, M.; Tsukanishi, K. Low dielectric material for multilayer printed wiring boards. IEEE Trans. Comp., Hybrids, Mfg. Technol. 13: 1115–1120; 1990 December.

[16] Jean, J. Ho; Gupta, T. K. Design of low dielectric glass+ceramics for multilayer ceramic substrate. IEEE Trans. Comp., Pkg., Mfg. Technol.:Part B 17: 228–233; 1994 May.

[17] Takahashi, H.; Ayusawa, K.; Sakamoto, N. Ba-Mg-Ti-O ceramics with temperature-stable low microwave loss. Jpn. J. Appl. Phys. 37: 908–911; 1998.

[18] Lee, H. Jong; Hong, K. Crystal structure and microwave dielectric properties of $M(Nb_xTa_{1-x})_2O_6$ and solid solution (M=Mg or Zn). J. Mater. Res. 12: 1437–1440; 1997 June.

[19] Azough, F.; Freer, R.; Wang, C. L.; Lorimer, G. W. The relationship between the microstructure and microwave dielectric properties of zirconium titanate ceramics. J. Mater. Sci. 31: 2539–2549; 1996.

[20] Davies, P. Influences of internal interfaces on the dielectric properties of ceramic microwave resonators. 357; 351–361; 1995.

[21] Valant, M.; Suvorov, D. New high-permittivity $AgNb_{1-x}Ta_xO_3$ microwave ceramics: Part I, crystal structures and phase-decomposition relations. J. Am. Ceram. Soc. 82: 81–87; 1999.

[22] Valant, M.; Suvorov, D. New high-permittivity $AgNb_{1-x}Ta_xO_3$ microwave ceramics: Part II, dielectric characteristics. J. Am. Ceram. Soc. 82: 88–93; 1999.

[23] Tummala, R. R. Multichip packaging: a tutorial. Proc., IEEE 80: 1924–1941; 1992 December.

[24] Weast, R. C. Handbook of Chemistry and Physics, 56th edition. Cleveland, OH: CRC Press; 1976.

[25] Tummala, R. R. Ceramic and glass-ceramic packaging in the 1990s. J. Am. Ceram. Soc. 74: 895–908; 1991.

[26] Kajfez, D.; Guillon, P. Dielectric Resonators. New York: ARCH HOUSE; 1986.

[27] Jean, J.Ho. Design of low dielectric glass+ceramics for multilayer ceramic substrates. IEEE Trans. Comp., Pkg., Mfg. Technol.:Part B 17: 228–233; 1994.

[28] Yeh, C.; Ume, C.; Fulton, R. E.; Wyatt, K. W.; Stafford, J. W. Correlation of analytical and experimental approaches to determine thermally induced pwb warpage. IEEE Trans. Comp., Hybrids, Mfg., Technol. 16: 986–994; 1993 December.

[29] ASTM-D3380-90 standard test method for relative permittivity and dissipation factor for polymer-based microwave circuit substrates. 1990 Annual Book of ASTM Standards 10.01; 1990.

[30] Microwave frequency dielectric properties of poly (vinylidene fluoride) films. J. Poly. Sci. 10.01; 1995.

[31] McPhun, M.; Mehmet, K. Thin film dielectric measurements; 60–71. IPC Science and Technology; Guilford, U.K.; 1973.

[32] Harrington, R. D.; Powell, R. C.; Haas, P. H. A re-entrant cavity for measurement of complex permeability in the very-high frequency region. J. Res. Nat. Bur. Stand.(U.S.) 56(3): 129–133; 1956.

[33] Works, C. N.; Dakin, T. W.; Boggs, F. W. A resonant cavity method for measuring dielectric properties at ultra-high frequencies. AIEE Trans. 63: 1092–1098; 1944.

[34] Baker-Jarvis, J.; Riddle, B. F. Dielectric measurements using a reentrant cavity. Natl. Inst. Stand. Technol. Tech. Note 1384; 1996 November.

[35] Kaczkowski, A.; Milewski, A. High-accuracy wide-range measurement method for determination of complex permittivity in re-entrant cavity: Part A, theoretical analysis of the method. IEEE Trans. Microwave Theory Tech. MTT-28(3): 225–228; 1980.

[36] Kaczkowski, A.; Milewski, A. High-accuracy wide-range measurement method for determination of complex permittivity in reentrant cavity, Part B- experimental analysis of measurement errors. IEEE Trans. Microwave Theory Tech. MTT-28(3): 228–231; 1980.

[37] Kent, G. Nondestructive measurements of substrate permittivity. Proc, of the 3rd International Symp. on Recent Advances in Microwave Technology; 1–4. ISRAMT'91; 1991.

[38] Kent, G. An evanescent-mode tester for ceramic dielectric substrates. IEEE Trans. Microwave Theory Tech. MTT-36; 1451–1454; 1988 October.

[39] Kent, G. A dielectrometer for the measurement of substrate permittivity. Microwave J.; 72–82; 1991 December.

[40] Janezic, M. D.; Baker-Jarvis, J. Full-mode model of split cavity resonator. IEEE Trans. Microwave Theory Tech., in press; 1998.

[41] Vanzura, E. J.; Baker-Jarvis, J. R.; Grosvenor, J. H.; Janezic, M. D. Intercomparison of permittivity measurements using the transmission/reflection method in 7-mm coaxial transmission lines. IEEE Trans. Microwave Theory Tech. MTT-42(11): 2063–2070; 1994 November.

[42] Damaskos, N. Measuring dielectric constants of low loss materials using a broadband cavity technique. Microwave J. 38: 140–147; 1995 September.

[43] Bussey, H. E.; Steinert, L. A. Exact solution for a gyromagnetic sample and measurements on a ferrite. IRE Trans. Microwave Theory Tech. MTT-6: 72–76; 1958 January.

[44] Kobayashi, Y.; Katoh, M. Microwave measurement of dielectric properties of low-loss materials by the dielectric rod resonator method. IEEE Trans. Microwave Theory Tech. MTT-33: 586–592; 1985.

[45] Nishikawa, T.; Tanaka, H.; Ishikawa, Y. Noncontact relative measurement method for complex permittivity of ceramic substrate. IECE of Japan Symposium Digest; 154–155; 1986.

[46] Maj, S.; Pospieszalski, M. A composite multilayered cylindrical dielectric resonator. MTT-S Digest; 190–192. IEEE; 1984 May.

[47] Delaballe, J. Complex permittivity measurement of MIC substrates. Electron. Telecommun. 35: 80–83; 1981.

[48] Krupka, J.; Baker-Jarvis, J.; Ceremuga, R. G. G. J. Measurement of the complex permittivity of microwave circuit board substrates using split dielctric resonator and reentrant cavity. Dielectric Materials Measurements and Applications; 21–24. IEE; 1996.

[49] Krupka, J.; Geyer, R. G. Complex permeability of demagnetized microwave ferrites near and above gyromagnetic resonance. IEEE Trans. Magn. 32: 1924–1933; 1996.

[50] Courtney, W. E. Analysis and evaluation of a method of measuring the complex permittivity and permeability of microwave insulators. IEEE Trans. Microwave Theory Tech. MTT-18: 467–485; 1970 August.

[51] Klein, N. Properties and applications of HTS-shielded dielectric resonators: a state-of the-art report. IEEE Trans. Microwave Theory Tech. 44: 1369–1373; 1996.

[52] Geyer, R.; Vanderah, T.; Jones, C.; Krupka, J. Complex permeability measurements of ferrite ceramics used in wireless communications. Ceram. Trans. 88: 93–111; 1998.

[53] Geyer, R.; Baker-Jarvis, J.; Vanderah, T.; Mantese, J. Complex permittivity and permeability estimation of composite electroceramics. Ceram. Trans. 88: 115–120; 1998.

[54] Krupka, J.; Derzakowski, F.; Modelski, J. Method of measuring the complex permittivity and permeability of ferrite substrate plates by means of two section dielectric resonator with TE01δ mode. MIKON Digest; 393–397; 1991 September.

[55] Lewis, R. L. Relative permittivity measurement of square copper-laminated substrates using the full-sheet resonance technique. Natl. Inst. Stand. Technol. NISTIR 5053; 1997.

[56] Woolaver, G. I. Accurately measure dielectric constant of soft substrates. Microwave & RF 24: 153–158; 1990 August.

[57] Weiming, O.; Gardner, C. G.; Long, S. A. Nondestructive measurement of a dielectric layer using surface electromagnetic waves. IEEE Trans. Microwave Theory Tech. MTT-31(3): 255–260; 1983 March.

[58] Krupka, J.; Blondy, P.; Cros, D.; Guillon, P.; Geyer, R. G. Whispering-gallery modes and permeability tensor measurements in magnetized ferrite resonators. IEEE Trans. Microwave Theory Tech. 44: 1097–1102; 1996.

[59] Krupka, J. Measurement of all permeability tensor components and effective linewidth of microwave ferrites using dielectric ring resonators. IEEE Trans. Microwave Theory Tech. 39: 1148–1157; 1991.

[60] Luiten, A. N.; Tobar, M.; Krupka, J.; Woode, R.; Ivanov, E. N.; Mann, A. G. Microwave properties of a rutile resonator between 2 and 10 k. J. Appl. Phys. 31: 1383–1391; 1998 June.

[61] Tobar, M.; Krupka, J.; Woode, R. A. Anisotropic complex permittivity measurements of mono-crystalline between 10 and 300 ^{o}K. J. Appl. Phys. 31: 1383–1391; 1998 June.

[62] Rayleigh, L. The problem of the whispering gallery. Phil. Mag. 20: 1001–1004; 1910.

[63] Wait, J. R. Electromagnetic whispering-gallery modes in a dielectric rod. Radio Sci. 2: 1005–1017; 1967.

[64] Vedrenne, C.; Arnaud, J. Whispering-gallery modes in dielectric resonators. IEE Proc. H. Microwave, Antennas, and Propagation 129: 183–187; 1982.

[65] Alexander, R. W.; Jr.; Bell, R. J. The use of surface electromagnetic waves to measure material properties. J. Noncryst. Solids 19: 93–103; 1975.

[66] Krupka, J.; Cros, D.; Aubourg, M.; Guillon, P. Study of whispering gallery modes in anisotropic single-crystal dielectric resonators. IEEE Trans. Microwave Theory Tech. 42(1): 56–61; 1994.

[67] Lynch, A. C. Precise measurement of complex permittivity and permeability in the millimeter region by a frequency domain technique. IEEE Trans. Instrum. Meas. 23: 425–430; 1974.

[68] Afsar, M. A. Dielectric measurements of millimeter-wave materials. IEEE Trans. Microwave Theory Tech. MTT-32(12): 1598–1609; 1984.

[69] Kogelnik, H.; Li, T. Laser beams and resonators. Proc., IEEE 54: 1312–1328; 1966.

[70] Jones, R. G. Precise dielectric measurements at 35 GHz using an open microwave resonator. IEE Proc. 123: 285–290; 1976.

[71] Clarke, R. N.; Rosenberg, C. B. Fabry-Perot and open resonators at microwave and millimeter wave frequencies, 2-300 GHz. J. Phys. E.: Sci. Instrum. 15(9): 9–24; 1982.

[72] Weir, W. B. Automatic measurement of complex dielectric constant and permeability at microwave frequencies. Proc., IEEE 62(1): 33–36; 1974 January.

[73] Baker-Jarvis, J. Transmission/reflection and short-circuit line permittivity measurements. Natl. Inst. Stand. Technol. Tech. Note 1341; 1990 July.

[74] Baker-Jarvis, J.; Vanzura, E.; Kissick, W. Improved technique for determining complex permittivity with the transmission/reflection method. IEEE Trans. Microwave Theory Tech. 38(8): 1096–1103; 1990 August.

[75] Goldfarb, R. B.; Bussey, H. E. Method for measuring complex permeability at radio frequencies. Rev. Sci. Instrum. 58(4): 624–627; 1987.

[76] Baker-Jarvis, J.; Geyer, R. G.; Domich, P. D. A nonlinear optimization technique for permittivity and permeability determination. IEEE Trans. Instrum. Meas. 41(5): 646–652; 1992.

[77] Mattar, K. E.; Watters, D. G.; Brodwin, M. E. Influence of wall contacts on measured complex permittivity spectra at coaxial line frequencies. IEEE Trans. Microwave Theory Tech. MTT-39(3): 532; 1991.

[78] York, R. A.; Compton, R. C. An automated method for dielectric constant measurements of microwave substrates. Microwave J. 33: 115–121; 1990 March.

[79] Traut, G. R. Electrical test methods for microwave pcb's. Microwave J. 24: 73–79; 1981 August.

[80] Howell, J. Q. A quick, accurate method to measure the dielectric constant of microwave integrated circuits. IEEE Trans. Microwave Theory Tech. MTT-21: 142–143; 1973 March.

[81] Napoli, L. S. A simple technique for the accurate determination of microwave dielectric constant for microwave integrated circuits. IEEE Trans. Microwave Theory Tech. MTT-19: 664–667; 1971 July.

[82] Gupta, K. C.; Garg, R.; Bahl, I. J. Microwave Lines and Slotlines. Norwood, MA: Artech House; 1979.

[83] Schneider, M. V. Microstrip lines for microwave integrated circuits. Bell Syst. Tech. J.; 1421–1444; 1968 May-June.

[84] Fidanboylu, K. M.; Riad, S. M.; Elshabini-Riad, A. A new time-domain approach for determining the complex permittivity using stripline geometry. IEEE Trans. Instrum. Meas. IM-39(6): 940–944; 1990 December.

[85] Waldron, R. A. Theory of a strip-line cavity for measurement of dielectric constants and gyromagnetic resonance line-widths. IEEE Trans. Microwave Theory Tech. IM-12: 123–131; 1964 January.

[86] Wheeler, H. A. Transmission-line properties of parallel-wide strips separated by a dielectric sheet. IEEE Trans. Microwave Theory Tech. MTT-13: 172–185; 1965 March.

[87] Getsinger, W. J. Microstrip dispersion model. IEEE Trans. Microwave Theory Tech. IM-21: 34–39; 1973 January.

[88] Bahl, I. J.; Stuchly, S. S. Analysis of a microstrip covered with a lossy dielectric. IEEE Trans. Microwave Theory Tech. MTT-28(2): 104–109; 1980 February.

[89] Tanaka, H.; Okada, F. Precise measurements of dissipation factor in microwave printed circuit boards. IEEE Trans. Instrum. Meas. IM-38(2): 509–514; 1989 April.

[90] Olyphant, M.; Ball, J. H. Stripline methods for dielectric measurements at microwave frequencies. IEEE Trans. Electron. Insul. EI-5(1): 26–32; 1970 March.

[91] Das, N. K.; Voda, S. M.; Pozar, D. M. Two methods for the measurement of substrate dielectric constant. IEEE Trans. Microwave Theory Tech. MTT-35: 636–641; 1987 July.

[92] Clapeau, M.; Guillon, P.; Garault, Y. Resonant frequencies of superimposed dielectric resonators: Application to determination of the local dielectric permittivity of mic substrates. Proc. 7th European Microwave Conf.; 545–549. EuMC'77; 1977.

[93] Laursen, K.; Hertling, D.; Berry, N.; Bidstrup, S. A.; Kohl, P.; Arroz, G. Measurement of the electrical properties of high performance dielectric materials for multichip modules. Proc., IEPS; 11–13; 1993. San Diego, CA.

[94] IPC-TM-650 test methods manual. The Institute for Interconnecting and Packaging Electronic Circuits 2.5.5.5; 1997.

[95] Gardiol, F. E.; Sphicopoulos, T.; Teodoridis, V. The reflection of open-ended circular waveguides: Application to nondestructive measurement of materials. Button, K. J., editor, Rev. Infrared Millimeter Waves; 325–364; New York; 1983. Plenum.

[96] Teodoridis, V.; Sphicopoulos, T.; Gardiol, F. E. The reflection from an open-ended rectangular waveguide terminated by a layered dielectric medium. IEEE Trans. Microwave Theory Tech. MTT-33(5): 359–366; 1985 May.

[97] Bringhurst, S.; Iskander, M. F. New metalized ceramic coaxial probe for high-temperature broadband dielectric properties of low permittivity materials. Microwaves: Theory and Application in Materials Processing II; 503–510. Amer. Ceram. Soc.: Ceramics Trans.; 1993.

[98] Li, L. L.; Ismail, N. H.; Taylor, L. S.; Davis, C. C. Flanged coaxial microwave probes for measuring thin moisture layers. IEEE Trans. Biomed. Eng. 39(1): 49–57; 1992 January.

[99] Langhe, P. D.; Blomme, K.; Martens, L.; Zutter, D. D. Measurement of low-permittivity materials based on a spectral domain analysis for the open-ended coaxial probe. IEEE Trans. Instrum. Meas. IM-42(9): 879–886; 1993 October.

[100] Levine, H.; Papas, C. H. Theory of the circular diffraction antenna. J. Appl. Phys. 22(1): 29–43; 1951 January.

[101] Baker-Jarvis, J.; Janezic, M. D.; Domich, P. D.; Geyer, R. G. Analysis of an open-ended coaxial probe with lift-off for nondestructive testing. IEEE Trans. Instrum. Meas.; 711–718; 1994 October.

[102] Hodgetts, T. E. The open-ended coaxial line: A rigorous variational treatment. Royal Signals and Radar Establishment 4331; 1989.

[103] Jenkins, S.; Hodgetts, T. E.; Symm, G. T.; Warhamm, A. G. P.; Clarke, R. N. Comparison of three numerical treatments for the open-ended coaxial line sensor. Electron. Lett. 26: 234–235; 1990.

[104] Ganchev, S.; Bakhtiari, S.; Zoughi, R. A novel numerical technique for dielectric measurements of lossy dielectrics. IEEE Trans. Instrum. Meas. 41: 361–365; 1992 June.

[105] Bussey, H. E. Measurement of rf properties of materials- a survey. Proc., IEEE 55(6): 1046–1053; 1967 June.

[106] Hartshorn, L.; Ward, W. H. The measurement of the permittivity and power factor of dielectrics at frequencies 10^4 to 10^8 cycles per second. J. Inst. Elec. Eng. 79: 597–609; 1936.

[107] Broadhurst, M. G.; Bur, A. J. Two-terminal dielectric measurements up to 6×10^8 Hz. J. Res. nat. Bur. Stand.(U.S.) 69C(3): 165–172; 1965.

[108] Jenkins, S.; Hodgetts, T. E.; Clarke, R. N.; Preece, A. W. Dielectric measurements on reference liquids using automatic network analyzers and calculable geometries. Meas. Sci. Tech. 1: 691–702; 1990.

[109] New technologies for wide impedance range measurements to 1.8 GHz. Hewlett Packard; 1994.

[110] ASTM-D1531: Relative permittivity and dissipation factor by fluid displacement procedures. 1990 Annual Book of ASTM Standards 10.02; 1990.

[111] Baker-Jarvis, J.; Geyer, R.; Grosvenor, J.; Janezic, M.; Jones, C.; Riddle, B.; Weil, C.; Krupka, J. Dielectric measurements on low-loss materials: A comparison of techniques. IEEE Trans. Dielect. and Insul. 5; 571–577; 1998 August.

[112] Vanzura, E. J.; Weil, C. M.; Williams, D. F. Complex permittivity measurements of gallium arsenide using a high-performance resonant cavity. CPEM'92 Digest; 103–104. Conference on Precision Electromagnetic Measurements; 1992.

[113] Bussey, H. E.; Gray, J. E.; Bamberger, E. C.; Rushton, E.; Russell, G.; Petley, B. W.; Morris, D. International comparison of dielectric measurements. IRE Trans. Instrum. Meas. IM-13(4): 305–311; 1964 December.

[114] Bussey, H. E.; Morris, D.; Zaltsman, E. B. International comparison of complex permittivity at 9 ghz. IEEE Trans. Instrum. Meas. IM-23(3): 235–238; 1974 September.

[115] Westphal, W. P.; Sils, A. Dielectric constant and loss data. MIT AFML-TR-72-39; 1972.

[116] Westphal, W. B. Dielectric constant and loss data. MIT AFML-TR-74-250; 1980.

*U.S. GPO -2000-0-573-020/40163

Contents

NIST Technical Note 1512

Dielectric and Magnetic Properties of Printed Wiring Boards and Other Substrate Materials

James Baker-Jarvis
Bill Riddle
Michael D. Janezic

Radio-Frequency Technology Division
Electronics and Electrical Engineering Laboratory
National Institute of Standards and Technology
325 Broadway
Boulder, Colorado 80303-3328

March 1999

U.S. DEPARTMENT OF COMMERCE, William M. Daley, Secretary
TECHNOLOGY ADMINISTRATION, Gary R. Bachula, Acting Under Secretary for Technology
NATIONAL INSTITUTE OF STANDARDS AND TECHNOLOGY, Raymond G. Kammer, Director